

Integrated Channel Estimation and Sensing for Near-Field ELAA Systems

Jionghui Wang, Jun Fang, Hongbin Li, *Fellow, IEEE* and Boyu Ning

Abstract—In this paper, we study the problem of uplink channel estimation for near-field orthogonal frequency division multiplexing (OFDM) systems, where a base station (BS), equipped with an extremely large-scale antenna array (ELAA), serves multiple users over the same time-frequency resource block. A non-orthogonal pilot transmission scheme is considered to accommodate a larger number of users that can be supported by ELAA systems without incurring an excessive amount of training overhead. To facilitate efficient multi-user channel estimation, we express the received signal as a third-order low-rank tensor, which admits a canonical polyadic decomposition (CPD) model for line-of-sight (LoS) scenarios and a block term decomposition (BTD) model for non-line-of-sight (NLoS) scenarios. An alternating least squares (ALS) algorithm and a non-linear least squares (NLS) algorithm are employed to perform CPD and BTD, respectively. Channel parameters are then efficiently extracted from the recovered factor matrices. By exploiting the geometry of the propagation paths in the estimated channel, users' positions can be precisely determined in LoS scenarios. Moreover, our uniqueness analysis shows that the proposed tensor-based joint multi-user channel estimation framework is effective even when the number of pilot symbols is much smaller than the number of users, revealing its potential in training overhead reduction. Simulation results demonstrate that the proposed method achieves markedly higher channel estimation accuracy than compressed sensing (CS)-based approaches.

I. INTRODUCTION

A. Background

Millimeter-wave (mmWave) and terahertz (THz) communications empowered by extremely large-scale antenna arrays (ELAA), which offer abundant spectrum resources and unprecedented spatial degrees of freedom (DoFs), are widely regarded as promising technologies for next-generation wireless communication systems [1]–[3]. As the array aperture increases and the carrier wavelength decreases, the Rayleigh distance can extend to tens or even hundreds of meters, shifting the propagation characteristics from far-field planar wavefronts to near-field spherical wavefronts [4], [5]. As a result, the channel response depends not only on the angle but also on the propagation distance. This additional range dimension enables distance-aware beam focusing and high spatial resolution, which are beneficial for both high-throughput communications and high-precision sensing [6], [7]. Consequently, mmWave/THz systems with ELAA have emerged as a

Jionghui Wang, Jun Fang and Boyu Ning are with the National Key Laboratory of Wireless Communications, University of Electronic Science and Technology of China, Chengdu 611731, China, Email: jionghuiwang@std.uestc.edu.cn;JunFang@uestc.edu.cn;boyning@outlook.com

Hongbin Li is with the Department of Electrical and Computer Engineering, Stevens Institute of Technology, Hoboken, NJ 07030, USA, E-mail: Hongbin.Li@stevens.edu

promising platform for integrated sensing and communication (ISAC), supporting various environment-aware applications, such as smart Internet of Things, autonomous driving, and extended reality [8], [9].

In ISAC systems, channel estimation and sensing can be naturally integrated by reusing the same transmitted signals. Specifically, during the channel state information (CSI) acquisition phase, pilot signals can be exploited not only to estimate channel coefficients, but also to extract key physical parameters of the propagation paths, such as direction of arrival (DoA), propagation distance, and time delay. These parameters can subsequently be leveraged for channel reconstruction and user localization. However, the integrated channel estimation and sensing in near-field regime is challenging, since the spherical wavefront exhibits a nonlinear structure, where the angle and distance parameters are strongly coupled.

B. Related Work

Near-field channel estimation and source localization have attracted extensive attention in both wireless communication and radar sensing systems.

For near-field channel estimation, the authors in [10] proposed a polar-domain sparse representation, where the dictionary is constructed by sampling over the two-dimensional (2D) angular-range domain. Based on the polar-domain codebook, near-field channel estimation can be formulated as a compressed sensing (CS) problem, which can be efficiently solved by a variety of methods [10]–[13]. Nevertheless, joint sampling over this 2D domain results in a dictionary with a large number of atoms, leading to high computational complexity. In [14], authors showed that near-field channels exhibit a block-sparse representation on a specially designed unitary matrix. This new representation leads to a well-conditioned measurement matrix that is more amiable for CS of near-field channels. In addition to CS-based methods, tensor decomposition-based methods were developed for far-field mmWave/THz channel estimation [15], [16] and later extended to near-field channel scenarios [17] by exploiting inherent multi-dimensional channel structures.

For near-field source localization, classical subspace-based approaches, such as multiple signal classification (MUSIC) and estimation of signal parameters by rotational invariance techniques (ESPRIT), have been extended to a variety of near-field variants to achieve high-resolution angle and distance estimation. In [18], the authors proposed a 2D-MUSIC algorithm that jointly estimate the angles and ranges via a 2D-grid search. However, such a grid search is computationally

intensive, especially when fine resolution is required. By exploiting the symmetric geometry of the antenna array, reduced-dimensional (RD) MUSIC and ESPRIT methods [19], [20] have been developed, where the angles are estimated via 1D-MUSIC/ESPRIT, and then the associated ranges can be calculated directly. Moreover, the near-field parameter estimation problem can also be formulated as a sparse reconstruction task, which can be solved by CS-based methods [21].

More recently, several studies have investigated integrated sensing and channel estimation in near-field ISAC systems. In [22], [23], joint user localization and channel estimation are achieved through the two-stage OMP-based algorithm. A tensor-based method is designed in [24], where the channel parameters are extracted from the tensor factor matrices using RD-MUSIC algorithm and correlation-based methods, enabling subsequent channel reconstruction and target localization.

However, most of the aforementioned works rely on the assumption that orthogonal pilot sequences are employed across users. Under this assumption, the multi-user channel estimation problem can be decoupled into a set of independent single-user subproblems. In practical systems, especially when a large number of users are simultaneously served or when the pilot length is severely limited, pilot orthogonality cannot be guaranteed. In such scenarios, non-orthogonal pilots lead to inevitable inter-user interference, and the received signals corresponding to different users become intrinsically coupled. Consequently, the multi-user channel estimation problem can no longer be decomposed into independent subproblems, and existing single-user near-field estimation methods [10]–[14], [17], [22]–[24] cannot be directly applied. Moreover, when the pilot length is smaller than the number of users, the received signal covariance matrix becomes rank-deficient, such that the dimension of the signal subspace is smaller than the number of users. This rank-deficiency violates the fundamental assumption of MUSIC/ESPRIT [18]–[20] that each steering vectors is orthogonal to the noise subspace. Therefore, conventional subspaced-based methods cannot be used without a prior user separation or decorrelation stage.

C. Contributions of This Work

In this paper, we investigate the problem of uplink joint multi-user channel estimation for near-field ELAA mmWave/THz OFDM systems. To accommodate a large number of users that can be supported by ELAA systems, we consider non-orthogonal uplink transmission scenarios where the length of pilot sequence is less than the number of served users. We model the received signal as a third-order tensor. Based on this model, we develop a tensor decomposition-based framework for channel parameter estimation. For the line-of-sight (LoS)-dominated scenario, the received signal is formulated as a third-order tensor that has a canonical polyadic decomposition (CPD) model, which is solved via an alternating least squares (ALS) algorithm. For the non-line-of-sight (NLoS) scenario, the formulated tensor follows a block term decomposition (BTD) model and the decomposition can be performed using a nonlinear least squares (NLS) algorithm.

The channel parameters and user association are then extracted from the resulting factor matrices using the correlation-based methods. In addition, we provide uniqueness analysis for both LoS and NLoS cases, showing that the multi-user channel parameters can be jointly and uniquely recovered as long as the pilot length satisfies $T \geq 2$. By exploiting the intrinsic geometry of the LoS paths, user locations can be precisely estimated. Simulations demonstrate that the proposed method significantly outperforms the CS-based baselines in channel estimation accuracy and achieves a high user localization precision.

Notations: a , \mathbf{A} and \mathcal{A} denote a vector, a matrix and a tensor, respectively; $(\cdot)^T$, $(\cdot)^H$, $(\cdot)^{-1}$ and $(\cdot)^\dagger$ denote the transpose, conjugate transpose, inverse and pseudo-inverse, respectively; $\mathbf{A}(:, m)$ and $\mathbf{A}(:, m : n)$ denote the m -th column of \mathbf{A} and the submatrix of \mathbf{A} from the m -th to the n -th columns, respectively; $\|\cdot\|_2$ and $\|\cdot\|_F$ denote the 2-norm and Frobenius norm, respectively; \otimes , \odot and \circ denote the Kronecker, Khatri-Rao and outer products, respectively; \mathbf{I}_n , $\mathbf{1}_m$, $\mathbf{0}_m$ and $\mathbf{0}_{m \times n}$ denote an $n \times n$ identity matrix, a $m \times 1$ all-ones vector, a $m \times 1$ all-zeros vector and a $m \times n$ all-zeros matrix, respectively; $\text{diag}(a_1, \dots, a_M)$ and $\text{blkdiag}(\mathbf{A}_1, \dots, \mathbf{A}_M)$ denote a $M \times M$ diagonal matrix with a_1, \dots, a_M placed along its diagonal and a block-diagonal matrix with matrices $\mathbf{A}_1, \dots, \mathbf{A}_M$ placed along its main diagonal, respectively; $\mathcal{U}(a, b)$ and $\mathcal{CN}(\mu, \sigma^2)$ denote a uniform distribution within range (a, b) and a complex Gaussian distribution with mean μ and variance σ^2 , respectively.

II. SYSTEM MODEL

We consider the problem of uplink channel estimation for ELAA mmWave/THz systems, as shown in Fig. 1, where the base station (BS), equipped with an extremely large-scale uniform linear array (ULA) with N antenna elements, serves a number of single-antenna users. We assume the system has a bandwidth of B Hz and consists of P sub-carriers. Let f_c denote the center carrier frequency, and the corresponding wavelength is $\lambda_c = c/f_c$, where c is the speed of light. The frequency associated with the p -th sub-carrier is expressed as $f_p = f_c + \frac{2p-P}{2P}B$, $p = 1, \dots, P$, with the corresponding wavelength given by $\lambda_p = c/f_p$.

The antenna spacing between two adjacent antennas at the BS is set to $d = \lambda_c/2$. Thus the array aperture and the Rayleigh distance are respectively given as $D = (N - 1)d$ and $d_R = \frac{2D^2}{\lambda_c}$. To balance the hardware cost and efficiency in mmwave/THz, we consider a hybrid analog and digital beamforming structure employed by the BS [25], where the number of radio frequency (RF) chains M is much less than the number of antenna elements but no smaller than the number of users, i.e., $K \leq M \ll N$.

A. Channel Model

As the number of antennas at the BS grows, the Rayleigh distance becomes comparable to the coverage radius. For example, for systems operating at 30 GHz, the Rayleigh distance d_R is around 80.6 meters for a half-wavelength ULA with $N = 128$ antennas. This implies that users are

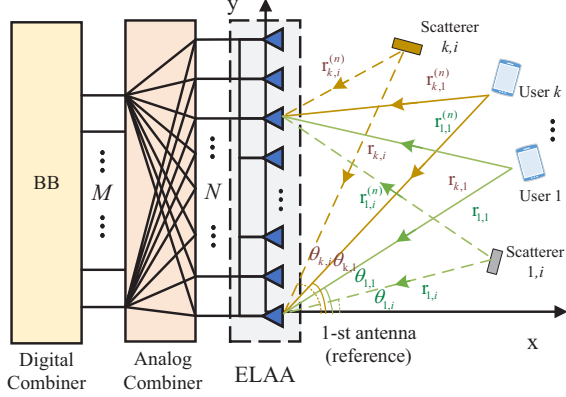


Fig. 1: An ELAA system with multiple users in the near-field.

highly likely located in the near-field region. In this case, the traditional planar wavefront model should be replaced by the more accurate spherical wavefront model. Specifically, the channel between the k -th user and the BS at the p -th sub-carrier can be characterized as

$$\mathbf{h}_{p,k} = \sum_{l=1}^{L_k} \alpha_{k,l} e^{-j2\pi f_p \tau_{k,l}} \mathbf{b}(\theta_{k,l}, r_{k,l}), \quad (1)$$

where L_k is the total number of signal paths between the BS and the k -th user; $\{\alpha_{l,k}, \tau_{l,k}, \theta_{l,k}, r_{l,k}\}$ respectively denote the complex channel gain, the time delay, the angle and the distance from the reference antenna to the user/scatterer associated with the l -th path; and $\mathbf{b}(\theta, r)$ is the near-field steering vector given by

$$\mathbf{b}(\theta, r) = \frac{1}{\sqrt{N}} [e^{-j\frac{2\pi}{\lambda}(r^{(1)}-r)} \dots e^{-j\frac{2\pi}{\lambda}(r^{(N)}-r)}]^T, \quad (2)$$

where $r^{(n)}$ denotes the distance between the user/scatterer and the n -th antenna of the BS. For simplicity, we choose the first antenna as the reference antenna and we have $r^{(1)} \equiv r$. According to the geometric relationship, $r^{(n)}$ can be written as

$$\begin{aligned} r^{(n)} &= \sqrt{r^2 + (n-1)^2 d^2 - 2r(n-1)d \sin \theta} \\ &\stackrel{(a)}{\approx} r - (n-1)d \sin \theta + \frac{(n-1)^2 d^2 \cos^2 \theta}{2r}, \end{aligned} \quad (3)$$

where (a) follows from the widely used Fresnel approximation [10]. Thus, the near-field steering vector $\mathbf{b}(\theta, r)$ can be further simplified as

$$\mathbf{b}(\theta, r) \approx \frac{1}{\sqrt{N}} [1 \dots e^{-j\frac{2\pi}{\lambda}(-(N-1)d \sin \theta + \frac{(N-1)^2 d^2 \cos^2 \theta}{2r})}]^T. \quad (4)$$

III. PROBLEM FORMULATION

In this paper, we consider the problem of uplink channel estimation and sensing based on the received pilot signal at the BS. Here “sensing” specifically means the localization of users based on the estimated near-field channel parameters. Note that the uplink channel estimation problem can be decomposed into

a number of parallel single-user channel estimation problems if different users utilize mutually orthogonal pilot sequences. Nevertheless, in this work, we consider a joint multi-user CPD-based channel estimation scheme, which uses non-orthogonal pilot sequences to accommodate a growing number of users in ELAA systems while avoiding excessive pilot overhead.

A. Received Signal Model

The training sequence consists of T consecutive OFDM symbols. At each time instant t , all users send their pilot vectors $\mathbf{s}_k[t] = [s_{1,k}[t] \ s_{2,k}[t] \ \dots \ s_{P,k}[t]]^T \in \mathbb{C}^P, \forall k$ to the BS, where $s_{p,k}[t]$ denotes the t -th pilot symbol associated with the k -th user and the p -th sub-carrier. Suppose that the pilots are common for all sub-carriers, i.e., $s_{p,k}[t] = s_k[t], \forall p$. At the BS, each RF chain, i.e., the m -th RF chain, employs an individual combining vector $\mathbf{w}_m \in \mathbb{C}^N$ to combine the received antenna signals. Considering the constant-modulus constraint imposed by analog beamforming, we assume that the BS adopts a random phase-only beamformer. Specifically, each entry of \mathbf{w}_m is generated as $w_{mn} = e^{j\Phi_{mn}}, \forall m, n$, where $\Phi_{mn} \sim \mathcal{U}(0, 2\pi)$ follows a uniform distribution. After analog combining, the cyclic prefix is removed and symbols are converted back to the frequency domain by performing a discrete Fourier transform (DFT). As a result, the received signal associated with the p -th sub-carrier and the m -th RF chain during the t -th time instant can be expressed as

$$\begin{aligned} y_{p,m}[t] &= \mathbf{w}_m^H \sum_{k=1}^K \mathbf{h}_{p,k} s_k[t] + \mathbf{w}_m^H \mathbf{n}_p[t] \\ &= \mathbf{w}_m^H \sum_{k=1}^K \sum_{i=1}^{L_k} \alpha_{k,i} e^{-j2\pi f_p \tau_{k,i}} \mathbf{b}(\theta_{k,i}, r_{k,i}) s_k[t] + \tilde{n}_{p,m}[t], \end{aligned} \quad (5)$$

where $\mathbf{h}_{p,k}$ represents the channel between the BS and the k -th user at the p -th sub-carrier; and $\tilde{n}_{p,m}[t] \triangleq \mathbf{w}_m^H \mathbf{n}_p[t]$ represents the effective additive white Gaussian noise (AWGN). For notation convenience, all propagation paths from different users are equivalently indexed by a single path index l . Specifically, by defining the mapping $l = \sum_{j=1}^{k-1} L_k + i$, we let $\alpha_l = \alpha_{k,i}$, $\theta_l = \theta_{k,i}$, $r_l = r_{k,i}$, and $\tau_l = \tau_{k,i}$. Moreover, the transmitted symbol associated with the l -th path is given by

$$\tilde{s}_l[t] = s_k[t], \quad \forall l \in \left[\sum_{i=1}^{k-1} L_k + 1, \sum_{i=1}^k L_k \right]. \quad (6)$$

Thus, the received signal corresponding to the p -th sub-carrier, the m -th RF chain and the t -th time instant can be re-written as

$$\begin{aligned} y_{p,m}[t] &= \mathbf{w}_m^H \sum_{l=1}^L \alpha_l e^{-j2\pi f_p \tau_l} \mathbf{b}(\theta_l, r_l) \tilde{s}_l[t] + \tilde{n}_{p,m}[t] \\ &= \sum_{l=1}^L g[p](\tau_l) \times a[m](\alpha_l, \theta_l, r_l) \times \tilde{s}_l[t] + \tilde{n}_{p,m}[t], \end{aligned} \quad (7)$$

where $L = \sum_{k=1}^K L_k$ denotes the total number of paths associated with all users; $g[p](\tau_l) \triangleq e^{-j2\pi f_p \tau_l}$ denotes the

frequency-domain phase response of the l -th path on the p -th subcarrier due to the time delay τ_l ; and $a[m](\alpha_l, \theta_l, r_l) \triangleq \alpha_l \mathbf{w}_m^H \mathbf{b}(\theta_l, r_l)$ represents the effective beamformed complex gain of the l -th path at the m -th RF chain, which jointly depends on the path gain α_l , angle θ_l , and range r_l .

B. Low-Rank Tensor Representation

To reveal the inherent multi-linear structure of the received signals across all the frequencies, RF chains, and time-instants, the received signal can be re-written as a third-order tensor $\mathcal{Y} \in \mathbb{C}^{P \times M \times T}$, whose (p, m, t) -th entry corresponds to $y_{p,m}[t]$. For the third-order tensor \mathcal{Y} , it is clear that the contribution from the l -th path can be represented as a rank-one tensor, which is the outer product of the following three vectors:

$$\begin{aligned} \mathbf{g}(\tau_l) &\triangleq [g[1](\tau_l) \cdots g[P](\tau_l)]^T \in \mathbb{C}^P, \\ \mathbf{a}(\alpha_l, \theta_l, r_l) &\triangleq [a[1](\alpha_l, \theta_l, r_l) \cdots a[M](\alpha_l, \theta_l, r_l)]^T \in \mathbb{C}^M, \\ \tilde{\mathbf{s}}_l &\triangleq [\tilde{s}_l[1] \cdots \tilde{s}_l[T]]^T \in \mathbb{C}^T. \end{aligned} \quad (8)$$

Consequently, the received tensor \mathcal{Y} admits a decomposition into a sum of rank-one component tensors, i.e.,

$$\mathcal{Y} = \sum_{l=1}^L \mathbf{g}(\tau_l) \circ \mathbf{a}(\alpha_l, \theta_l, r_l) \circ \tilde{\mathbf{s}}_l + \mathcal{N}, \quad (9)$$

where $\mathcal{N} \in \mathbb{C}^{P \times M \times T}$ denotes the noise tensor, whose (p, m, t) -th entry corresponds to $\tilde{n}_{p,m}[t]$. The tensor decomposition in (9) is known as the CPD. By collecting the factor vectors associated with all L propagation paths, we obtain the factor matrices associated with the noiseless part of \mathcal{Y} :

$$\begin{aligned} \mathbf{G} &\triangleq [\mathbf{g}(\tau_1) \cdots \mathbf{g}(\tau_L)] \in \mathbb{C}^{P \times L}, \\ \mathbf{A} &\triangleq [\mathbf{a}(\alpha_1, \theta_1, r_1) \cdots \mathbf{a}(\alpha_L, \theta_L, r_L)] \in \mathbb{C}^{M \times L}, \\ \mathbf{S} &\triangleq [\tilde{\mathbf{s}}_1 \cdots \tilde{\mathbf{s}}_L] \in \mathbb{C}^{T \times L}. \end{aligned} \quad (10)$$

Here, the factor matrix \mathbf{G} is characterized by different propagation delays across all subcarriers, \mathbf{A} captures complex path losses and near-field spatial responses associated with different paths, and \mathbf{S} is a matrix with its column corresponding to a certain user's pilot sequence.

The tensor form (9) of the received signals allows us to find an efficient way to estimate the wireless channel. Under certain mild uniqueness conditions, the received tensor \mathcal{Y} admits an essentially unique decomposition, up to scaling and permutation ambiguities. Thus we can first estimate the three factor matrices and then extract the associated channel parameters $\{\tau_l, \theta_l, r_l, \alpha_l\}_{l=1}^L$ from the recovered factor matrices. Specifically, the exact tensor decomposition model and the corresponding uniqueness conditions depend on the underlying channel propagation structure. In view of this, we discuss channel estimation for the LoS-dominated and NLoS scenarios in Sections IV and V, respectively.

IV. CHANNEL ESTIMATION FOR LOS-DOMINATED SCENARIOS

In this section, we first consider the scenario where the line-of-sight (LoS) path between the BS and each user is not

blocked. In mmWave/THz communication systems, the energy of NLoS paths is typically much smaller than that of the LoS path¹, making their contribution to the received signal negligible. Therefore, only the LoS path is modeled in this work for simplicity. In this case, we have $L = K$ and the received signal can be expressed as

$$\mathcal{Y} = \sum_{k=1}^K \mathbf{g}(\tau_k) \circ \mathbf{a}(\alpha_k, \theta_k, r_k) \circ \mathbf{s}_k + \mathcal{N}, \quad (11)$$

which admits a CPD with the following factor matrices:

$$\begin{aligned} \mathbf{G}_o &\triangleq [\mathbf{g}(\tau_1) \cdots \mathbf{g}(\tau_K)] \in \mathbb{C}^{P \times K}, \\ \mathbf{A}_o &\triangleq [\mathbf{a}(\alpha_1, \theta_1, r_1) \cdots \mathbf{a}(\alpha_K, \theta_K, r_K)] \in \mathbb{C}^{M \times K}, \\ \mathbf{S}_o &\triangleq [\mathbf{s}_1 \cdots \mathbf{s}_K] \in \mathbb{C}^{T \times K}. \end{aligned} \quad (12)$$

where $\mathbf{s}_k \triangleq [s_k[1] \cdots s_k[T]]^T$.

A. Uniqueness Condition

Before proceeding to the CPD, we first discuss under what conditions the uniqueness of the CPD can be guaranteed. A well-known sufficient condition is Kruskal's condition [27], which is stated in Theorem 1.

Theorem 1: Let k_A denote the k-rank of \mathbf{A} , which is defined as the maximum number k_A such that any k_A columns of \mathbf{A} are linearly independent. Let $(\mathbf{A}, \mathbf{B}, \mathbf{C})$ be a CP solution which decomposes a third-order tensor $\mathcal{Y} \in \mathbb{C}^{I_1 \times I_2 \times I_3}$ into Q rank-one components, where $\mathbf{A} \in \mathbb{C}^{I_1 \times Q}$, $\mathbf{B} \in \mathbb{C}^{I_2 \times Q}$, $\mathbf{C} \in \mathbb{C}^{I_3 \times Q}$. If the Kruskal condition

$$k_A + k_B + k_C \geq 2Q + 2 \quad (13)$$

is satisfied, then the CPD of \mathcal{Y} is unique up to scaling and permutation ambiguities. Specifically, the scaling and permutation ambiguities may lead to an alternative CP solution $(\bar{\mathbf{A}}, \bar{\mathbf{B}}, \bar{\mathbf{C}})$, which also decomposes \mathcal{Y} into Q rank-one components and it satisfies $\bar{\mathbf{A}} = \mathbf{A}\Lambda_A\Pi$, $\bar{\mathbf{B}} = \mathbf{B}\Lambda_B\Pi$, and $\bar{\mathbf{C}} = \mathbf{C}\Lambda_C\Pi$, where Λ_A , Λ_B and Λ_C are unique diagonal matrices such that $\Lambda_A\Lambda_B\Lambda_C = \mathbf{I}_Q$, and Π is a unique permutation matrix.

From the above theorem, the CPD of \mathcal{Y} is essentially unique if the following Kruskal condition is satisfied

$$k_{\mathbf{G}_o} + k_{\mathbf{A}_o} + k_{\mathbf{S}_o} \geq 2K + 2. \quad (14)$$

We next examine the k-ranks of the involved factor matrices.

We first consider the k-rank of \mathbf{G}_o . Since \mathbf{G}_o is a columnwise-scaled Vandermonte matrix characterized by distinct delay parameters $\{\tau_l\}$, the k-rank of \mathbf{G}_o is equal to the smallest value of P and K , i.e.,

$$k_{\mathbf{G}_o} = \min(P, K). \quad (15)$$

In practical OFDM systems, it is reasonable to assume that the number of sub-carriers allocated for training is greater than the number of users, i.e. $P \geq K$. Under this condition, we have $k_{\mathbf{G}_o} = K$.

¹Many channel measurement campaigns reveal that the power of the mmWave/THz LoS path is much higher (about 13 dB higher over the mmWave band and 20 dB higher over the THz band) than the sum of power of NLoS paths [26].

We now turn to the k-rank of \mathbf{A}_o . Recall that the factor matrix \mathbf{A}_o is obtained by projecting the weighted near-field steering vectors onto a reduced-dimensional RF domain through the analog combining matrix \mathbf{W} , i.e., $\mathbf{A}_o \triangleq \mathbf{W}^H \mathbf{B} \mathbf{D}_\alpha$, where

$$\begin{aligned}\mathbf{W} &\triangleq [\mathbf{w}_1 \cdots \mathbf{w}_M] \in \mathbb{C}^{N \times M}, \\ \mathbf{D}_\alpha &\triangleq \text{diag}\{\alpha_1, \dots, \alpha_K\} \in \mathbb{C}^{K \times K}, \\ \mathbf{B} &\triangleq [\mathbf{b}(\theta_1, r_1) \cdots \mathbf{b}(\theta_K, r_K)] \in \mathbb{C}^{N \times K},\end{aligned}\quad (16)$$

Generally, steering vectors with distinct angle-distance pairs are linearly independent with high probability [10]. Consequently, the near-field array response matrix \mathbf{B} is full column rank when $K \leq N$. Note that \mathbf{D}_α is a non-singular diagonal matrix. Hence $\mathbf{B}_\alpha \triangleq \mathbf{B} \mathbf{D}_\alpha$ is full column rank. As a result, the k-rank of \mathbf{A}_o depends on whether the RF-domain projection \mathbf{W}^H preserves the rank of \mathbf{B}_α .

Recall that a random phase-only combining matrix \mathbf{W} is employed, under which \mathbf{W} is full column rank with probability one. For any subset of k_{A_o} columns from \mathbf{B}_α (where $k_{A_o} \leq K$), their linear independence is preserved after projection if none of the linear combinations of these k_{A_o} columns lies in the null space of \mathbf{W}^H . Since entries of \mathbf{W}^H are randomly generated, the probability that the linear combination of these k_{A_o} columns lies in the null space of \mathbf{W}^H is zero, provided that $k_{A_o} \leq M$. As a result, with probability one, any subset of at most $\min\{M, K\}$ columns of \mathbf{A}_o is linearly independent, which implies that the k-rank of \mathbf{A}_o satisfies

$$k_{A_o} = \min\{M, K\} = K. \quad (17)$$

Based on the above results, we know that the Kruskal condition in (14) can be satisfied by designing a set of training sequences \mathbf{S}_o such that $k_{S_o} \geq 2$, namely, any two columns of \mathbf{S}_o are linearly independent. This condition can be readily met when $T \geq 2$ and the pilot vectors of different users are linearly independent. To be concrete, we can design the training pilots by minimizing the mutual coherence of \mathbf{S}_o , i.e.,

$$\min_{\mathbf{S}_o} \max_{i \neq j} \frac{|\mathbf{s}_i^H \mathbf{s}_j|}{\|\mathbf{s}_i\|_2 \|\mathbf{s}_j\|_2}, \quad (18)$$

where \mathbf{s}_i denotes the training pilot vector associated with the i -th user. This optimization is fundamentally a Grassmannian line packing problem [28], which aims to find a set of lines in a complex space that are as far apart as possible.

The aforementioned analysis reveals that the proposed CPD framework ensures the uniqueness of the channel decomposition even in the underdetermined regime where $T \ll K$ (provided that $T \geq 2$). As a result, all users' channels can be jointly estimated without requiring $T = K$ orthogonal pilot sequences to decouple the multiuser channel estimation problem into a set of single-user channel estimation problems.

It should be noted that a minimum of $T = 2$ OFDM pilot symbols are required to satisfy the CPD uniqueness condition, provided that the pilot sequences corresponding to different users are linearly independent. When the number of users becomes excessively large, setting $T = 2$ may result in a weak linear independence among pilot sequences, and the uniqueness condition barely holds valid. In such cases, a

larger value of T may be necessary. Nevertheless, compared to conventional orthogonal pilot-based schemes, the proposed method can still substantially reduce the training overhead by setting the number of OFDM pilot symbols much smaller than the number of users. Such a merit is particularly attractive in scenarios with a large number of users.

B. CP Decomposition

The CPD can be accomplished by solving the following optimization problem

$$\min_{\mathbf{G}_o, \mathbf{A}_o, \mathbf{S}_o} \left\| \mathcal{Y} - \sum_{k=1}^K \hat{\mathbf{g}}_k \circ \hat{\mathbf{a}}_k \circ \hat{\mathbf{s}}_k \right\|_F^2. \quad (19)$$

Here, the number of users K is known *a priori*, and $\hat{\mathbf{g}}_k$, $\hat{\mathbf{a}}_k$ and $\hat{\mathbf{s}}_k$ denote the k -th column of \mathbf{G}_o , \mathbf{A}_o and \mathbf{S}_o , respectively. The above optimization can be efficiently solved by an ALS procedure, which iteratively minimizes the data fitting error with respect to (w.r.t.) the three factor matrices:

$$\mathbf{G}_o^{(t+1)} = \arg \min_{\mathbf{G}_o} \left\| \mathbf{Y}_{(1)}^T - (\mathbf{S}_o^{(t)} \odot \mathbf{A}_o^{(t)}) \mathbf{G}_o^T \right\|_F^2, \quad (20)$$

$$\mathbf{A}_o^{(t+1)} = \arg \min_{\mathbf{A}_o} \left\| \mathbf{Y}_{(2)}^T - (\mathbf{S}_o^{(t)} \odot \mathbf{G}_o^{(t+1)}) \mathbf{A}_o^T \right\|_F^2, \quad (21)$$

$$\mathbf{S}_o^{(t+1)} = \arg \min_{\mathbf{S}_o} \left\| \mathbf{Y}_{(3)}^T - (\mathbf{A}_o^{(t+1)} \odot \mathbf{G}_o^{(t+1)}) \mathbf{S}_o^T \right\|_F^2, \quad (22)$$

where $\mathbf{Y}_{(n)}$, $n = 1, 2, 3$ denotes the mode- n unfolding of the tensor \mathcal{Y} .

As discussed earlier, the CPD is unique up to scaling and permutation ambiguities under some mild conditions. Specifically, the relationship between the estimated factor matrices and the true factor matrices is given by

$$\begin{aligned}\hat{\mathbf{G}}_o &= \mathbf{G}_o \mathbf{\Lambda}_1 \mathbf{\Pi} + \mathbf{E}_1, \\ \hat{\mathbf{A}}_o &= \mathbf{A}_o \mathbf{\Lambda}_2 \mathbf{\Pi} + \mathbf{E}_2, \\ \hat{\mathbf{S}}_o &= \mathbf{S}_o \mathbf{\Lambda}_3 \mathbf{\Pi} + \mathbf{E}_3,\end{aligned}\quad (23)$$

where $\mathbf{\Lambda}_1$, $\mathbf{\Lambda}_2$ and $\mathbf{\Lambda}_3$ are nonsingular diagonal matrices and satisfy $\mathbf{\Lambda}_1 \mathbf{\Lambda}_2 \mathbf{\Lambda}_3 = \mathbf{I}$; $\mathbf{\Pi}$ is a permutation matrix; \mathbf{E}_1 , \mathbf{E}_2 and \mathbf{E}_3 denote the estimation errors associated with the three estimated factor matrices, respectively.

C. Channel Estimation

We now discuss how to extract the channel parameters from the estimated factor matrices. Ignoring the estimation errors \mathbf{E}_3 , it can be observed that each column of $\hat{\mathbf{S}}_o$ is a scaled version of a training sequence associated with a certain user. Note that all available training pilots are known *a priori* at the BS. Hence, the permutation matrix $\mathbf{\Pi}$ can be estimated via a simple correlation-based method. More precisely, the user index associated with the k -th column of $\hat{\mathbf{S}}_o$ can be estimated as

$$\hat{i}_k = \arg \max_{i \in \{1, \dots, K\}} \frac{|\mathbf{s}_i^H \hat{\mathbf{s}}_k|}{\|\mathbf{s}_i\|_2 \|\hat{\mathbf{s}}_k\|_2}, \quad \forall k = 1, \dots, K, \quad (24)$$

If more than two columns choose the same user index, there exists a conflict. The column with a higher correlation retains this index, while the other column chooses a new index from

the remaining indices by repeating (24). After determining the user index associated with each column, the permutation matrix Π can be obtained as

$$\Pi(i, j) = \begin{cases} 1, & (i, j) \in \{(i_k, k)\}_{k=1}^K, \\ 0, & \text{otherwise.} \end{cases} \quad (25)$$

Given Π , the permutation ambiguity for the estimated factor matrices can be removed. Thus, we have

$$\begin{aligned} \hat{\mathbf{G}}_o &= \hat{\mathbf{G}}_o \Pi^T = \mathbf{G}_o \Lambda_1 + \mathbf{E}_1, \\ \hat{\mathbf{A}}_o &= \hat{\mathbf{A}}_o \Pi^T = \mathbf{A}_o \Lambda_2 + \mathbf{E}_2, \\ \hat{\mathbf{S}}_o &= \hat{\mathbf{S}}_o \Pi^T = \mathbf{S}_o \Lambda_3 + \mathbf{E}_3, \end{aligned} \quad (26)$$

We can see that the k -th column of $\hat{\mathbf{G}}_o$ is a scaled version of $\mathbf{g}(\tau_k)$. Therefore, the delay parameter τ_k associated with the k -th user can be estimated by maximizing the normalized correlation

$$\eta_k(\tau) = \frac{|\mathbf{g}^H(\tau) \hat{\mathbf{g}}_k|}{\|\mathbf{g}(\tau)\|_2 \|\hat{\mathbf{g}}_k\|_2} \quad (27)$$

Instead of performing a single high-resolution line search, which may be computationally expensive, we adopt a two-stage coarse–fine search strategy. First, a coarse grid \mathcal{T}_c is used to obtain a rough estimate

$$\hat{\tau}_k^{(0)} = \arg \max_{\tau \in \mathcal{T}_c} \eta_k(\tau). \quad (28)$$

Then, a finer local search \mathcal{T}_f is conducted around $\hat{\tau}_k^{(0)}$ with a much smaller step size, yielding the final estimate

$$\hat{\tau}_k = \arg \max_{\tau \in \mathcal{T}_f} \eta_k(\tau). \quad (29)$$

Similarly, the k -th column of $\hat{\mathbf{A}}_o$ is a scaled version of $\tilde{\mathbf{b}}(\theta_k, r_k)$. By constructing a near-field codebook jointly sampled over the angle-range domain, the pair (r_k, θ_k) can also be estimated by a two-stage coarse–fine search, i.e.,

$$\hat{\theta}_k, \hat{r}_k = \arg \max_{\theta, r} \frac{|\mathbf{b}^H(\theta, r) \mathbf{W} \hat{\mathbf{a}}_k|}{\|\mathbf{W}^H \mathbf{b}(\theta, r)\|_2 \|\hat{\mathbf{a}}_k\|_2}, \quad (30)$$

The coarse search provides an initial estimate $(\hat{r}_k^{(0)}, \hat{\theta}_k^{(0)})$, and then a refined local search around it provides the final estimate $(\hat{r}_k, \hat{\theta}_k)$.

Moreover, in the LoS scenario, the time delay τ_k and the distance r_k satisfy a deterministic relationship, i.e. $\tau_k = r_k/c$. Hence, the distance from the BS to the k -th user can be directly obtained as $\hat{r}_k = \hat{\tau}_k c$. With \hat{r}_k readily determined, only the angle θ_k needs to be estimated through a two-stage coarse–fine search, i.e.

$$\theta_k = \arg \max_{\theta} \frac{|\mathbf{b}^H(\theta, \hat{r}_k) \mathbf{W} \hat{\mathbf{a}}_k|}{\|\mathbf{W}^H \mathbf{b}(\theta, \hat{r}_k)\|_2 \|\hat{\mathbf{a}}_k\|_2}, \quad (31)$$

Leveraging this prior relationship significantly reduces the computational complexity and improves the estimation accuracy, as it eliminates the joint range-angle search.

Next, we try to recover the path loss gains $\{\hat{\alpha}_k\}$. After obtaining $\{\hat{\tau}_k, \hat{\theta}_k, \hat{r}_k\}$, we can reconstruct

$$\begin{aligned} \tilde{\mathbf{G}}_o &= [\mathbf{g}(\hat{\tau}_1) \cdots \mathbf{g}(\hat{\tau}_K)], \\ \tilde{\mathbf{B}}_o &= \mathbf{W}^H [\mathbf{b}(\hat{\theta}_1, \hat{r}_1) \cdots \mathbf{b}(\hat{\theta}_K, \hat{r}_K)]. \end{aligned} \quad (32)$$

Ignoring the estimation error, the scaling ambiguity matrix can be estimated as $\Lambda_1 = \tilde{\mathbf{G}}_o^\dagger \tilde{\mathbf{G}}_o$ and $\Lambda_3 = \tilde{\mathbf{S}}_o^\dagger \mathbf{S}_o$. Moreover, since $\Lambda_1 \Lambda_2 \Lambda_3 = \mathbf{I}$, we have $\Lambda_2^\dagger = \Lambda_1 \Lambda_3$. Ideally, there should be $\hat{\mathbf{A}}_o = \tilde{\mathbf{B}}_o \mathbf{D}_a \Lambda_2$. Hence, \mathbf{D}_a can be estimated as

$$\hat{\mathbf{D}}_a = \text{diag}(\tilde{\mathbf{B}}_o^\dagger \hat{\mathbf{A}}_o \Lambda_1 \Lambda_3). \quad (33)$$

Finally, the channels $\{\mathbf{h}_{p,k}\}$ can be reconstructed by the estimated parameters $\{\hat{\tau}_k, \theta_k, \hat{r}_k, \hat{\alpha}_k\}$. With the obtained distance and angle information, the position of the k -th user is estimated as

$$\hat{\mathbf{p}}_k = [\hat{r}_k \cos \hat{\theta}_k, \hat{r}_k \sin \hat{\theta}_k]^T. \quad (34)$$

V. CHANNEL ESTIMATION FOR NLOS SCENARIOS

In this section, we discuss how to estimate the wireless channel for the general geometric multi-path scenario where the LoS path is blocked and there exists multiple NLoS paths between the BS and each user.

A. CPD Model and Uniqueness Analysis

In the NLoS scenario, the received signal still follows the general CPD model introduced in Eq. (9), where each propagation path contributes a rank-one component to the received signal tensor. Therefore, the noiseless part of received signal can be compactly characterized by the factor matrices defined in (10). Note that in \mathbf{S} , columns associated with the same user are identical. Therefore, the factor matrices \mathbf{S} can be further factorized as

$$\mathbf{S} \triangleq \mathbf{S}_o \mathbf{O}, \quad (35)$$

where \mathbf{S}_o and \mathbf{s}_k are defined in (12) and $\mathbf{O} \in \mathbb{B}^{K \times L}$ is a binary mapping matrix that associates each path with its corresponding user. Specifically, the (k, l) -th entry of \mathbf{O} is given by

$$o_{kl} = \begin{cases} 1, & l\text{-th path is associated with the } k\text{-th user,} \\ 0, & \text{otherwise,} \end{cases} \quad (36)$$

As a result, the k -th row of \mathbf{O} contains exactly L_k nonzero entries.

We next discuss the uniqueness condition of the CPD model in (9) for NLoS scenarios. Base on the theorem 1, Kruskal's condition for the general multi-path cases becomes

$$k_G + k_B + k_S \geq 2L + 2. \quad (37)$$

Since both the factor matrices $\mathbf{G} \in \mathbb{C}^{P \times L}$ and $\mathbf{A} \in \mathbb{C}^{M \times L}$ have a k-rank bounded by L , satisfying the above Kruskal condition strictly requires $k_S \geq 2$. However, this is unattainable in multi-path scenarios, where the path components associated with a common user share the same pilot sequence, rendering the k-rank of \mathbf{S} equal to one. As a result, Kruskal's condition under a CPD model can never be satisfied for the general multi-path scenario. This implies that if we still treat the received signal as a CPD model, the decomposition is not unique. The estimated factor matrices will suffer from severe rotational ambiguities, making it impossible to uniquely identify the parameters of individual paths.

B. BTD Model and Uniqueness Analysis

To resolve this issue, we aggregate the collinear components associated with the same user into a block term, rather than treat them as L_k independent rank-1 path components. As such, the received signal in (9) is reformulated as a BTD structure,

$$\begin{aligned}\mathcal{Y} &= \sum_{k=1}^K \sum_{i=1}^{L_k} \mathbf{g}(\tau_{k,i}) \circ \mathbf{a}(\alpha_{k,i}, \theta_{k,i}, r_{k,i}) \circ \mathbf{s}_k + \mathcal{N} \\ &= \sum_{k=1}^K (\mathbf{G}_k \mathbf{A}_k^T) \circ \mathbf{s}_k + \mathcal{N},\end{aligned}\quad (38)$$

where

$$\begin{aligned}\mathbf{G}_k &\triangleq [\mathbf{g}(\tau_{k,1}) \cdots \mathbf{g}(\tau_{k,L_k})], \\ \mathbf{A}_k &\triangleq [\mathbf{a}(\alpha_{k,1}, \theta_{k,1}, r_{k,1}) \cdots \mathbf{a}(\alpha_{k,L_k}, \theta_{k,L_k}, r_{k,L_k})],\end{aligned}\quad (39)$$

and \mathbf{s}_k is defined after (12). In this formulation, the tensor \mathcal{Y} is expressed as a sum of matrix-vector outer products, more specifically, a sum of rank- $(L_k, L_k, 1)$ terms since \mathbf{G}_k and \mathbf{A}_k are both rank- L_k . The generalized Kruskal's condition provides sufficient conditions for the uniqueness of the above BTD [29], which can be elaborated as follows.

Theorem 2: Let $(\mathbf{A}, \mathbf{B}, \mathbf{C})$ be a BTD solution which decomposes a third-order tensor $\mathcal{Y} \in \mathbb{C}^{I_1 \times I_2 \times I_3}$ into Q rank- $(L_q, L_q, 1)$ terms, i.e.

$$\mathcal{Y} = \sum_{q=1}^Q (\mathbf{A}_q \mathbf{B}_q^T) \circ \mathbf{c}_q, \quad (40)$$

where $\mathbf{A}_q \in \mathbb{C}^{I_1 \times L_q}$, $\mathbf{B}_q \in \mathbb{C}^{I_2 \times L_q}$ and $\mathbf{c}_q \in \mathbb{C}^{I_3}$ are the factor matrices/vectors associated with the q -th block term. Here we define $\mathbf{A} = [\mathbf{A}_1 \cdots \mathbf{A}_Q] \in \mathbb{C}^{I_1 \times L}$, $\mathbf{B} = [\mathbf{B}_1 \cdots \mathbf{B}_Q] \in \mathbb{C}^{I_2 \times L}$ and $\mathbf{C} = [\mathbf{c}_1 \cdots \mathbf{c}_Q] \in \mathbb{C}^{I_3 \times Q}$ with $L = \sum_{q=1}^Q L_q$. Moreover, we assume $I_1 \geq \max_q L_q$, $I_2 \geq \max_q L_q$, $\text{rank}(\mathbf{A}_q) = L_q$ and $\text{rank}(\mathbf{B}_q) = L_q$. If the following conditions

$$I_1 I_2 \geq \sum_{q=1}^Q L_q^2, \quad (41)$$

$$k_A' + k_B' + k_C \geq 2Q + 2, \quad (42)$$

are satisfied, then this BTD of \mathcal{Y} is unique up to scaling and permutation ambiguities.

Remark 1: Note that k_A' is the generalized k-rank concept of the concatenated matrix \mathbf{A} , which is defined as the maximal number k_A' such that any set of k_A' submatrices of \mathbf{A} yields a set of linearly independent columns.

Remark 2: Specifically, if there exists an alternative BTD solution $(\bar{\mathbf{A}}, \bar{\mathbf{B}}, \bar{\mathbf{C}})$ which also decomposes \mathcal{Y} into Q rank- $(L_q, L_q, 1)$ terms, then we have $\bar{\mathbf{A}} = \mathbf{A} \boldsymbol{\Lambda}_A \boldsymbol{\Pi}$, $\bar{\mathbf{B}} = \mathbf{B} \boldsymbol{\Lambda}_B \boldsymbol{\Pi}$, and $\bar{\mathbf{C}} = \mathbf{C} \boldsymbol{\Lambda}_C \boldsymbol{\Pi}_C$, where $\boldsymbol{\Pi}$ is a Q -block permutation matrix; $\boldsymbol{\Pi}_C$ is a permutation matrix whose permutation pattern is the same as that of $\boldsymbol{\Pi}$; $\boldsymbol{\Lambda}_A$ and $\boldsymbol{\Lambda}_B$ are nonsingular Q -block diagonal matrices; $\boldsymbol{\Lambda}_C$ is a nonsingular diagonal matrix. Note that the block structure of $\boldsymbol{\Pi}$, $\boldsymbol{\Lambda}_A$ and $\boldsymbol{\Lambda}_B$ is compatible with that of \mathbf{A} and \mathbf{B} . Let $\boldsymbol{\Lambda}_{A,q}$ and $\boldsymbol{\Lambda}_{B,q}$ denote the q -th diagonal block of $\boldsymbol{\Lambda}_A$ and $\boldsymbol{\Lambda}_B$, respectively, and λ_q denote the q -th diagonal element of $\boldsymbol{\Lambda}_C$. Then, we have $\lambda_q \boldsymbol{\Lambda}_{A,q} \boldsymbol{\Lambda}_{B,q}^T = \mathbf{I}_{L_q}, \forall q$.

According to Theorem 2, the essential uniqueness of the BTD formulation in (38) is guaranteed if the following two sufficient conditions are met

$$PM \geq \sum_{k=1}^K L_k^2, \quad (43)$$

$$k_G' + k_A' + k_{S_o} \geq 2K + 2. \quad (44)$$

The first dimensionality constraint (43) is generally non-restrictive in mmWave/THz ELAA systems, since the number of paths is usually small relative to the other two dimensions. Following an analysis similar to that in the previous section, we can arrive at $k_G' = K$ and $k_A' = K$ with probability one. Substituting this into (44), the uniqueness condition reduces to $k_{S_o} \geq 2$, which can be easily satisfied by designing pairwise independent training sequences associated with different users (provided that $T \geq 2$).

C. BT Decomposition

The BTD can be accomplished by solving the following optimization problem

$$\min_{\{\mathbf{G}_k, \mathbf{A}_k, \mathbf{s}_k\}} \frac{1}{2} \left\| \mathcal{Y} - \sum_{k=1}^K (\hat{\mathbf{G}}_k \hat{\mathbf{A}}_k^T) \circ \hat{\mathbf{s}}_k \right\|_F^2. \quad (45)$$

Here, the number of users and the number of paths associated with each user are assumed known *a priori*. The above problem can be efficiently solved by the non-linear least squares (NLS) algorithm implemented in Tensorlab [30], which jointly updates all factor matrices in an iterative manner by exploiting the Jacobian structure of the tensor model, typically using a Gauss-Newton [31] or Levenberg-Marquardt (LM) strategy [32]. To be concrete, the problem (45) can be re-written as

$$\min_{\mathbf{m}} \frac{1}{2} \boldsymbol{\mu}^H(\mathbf{m}) \boldsymbol{\mu}(\mathbf{m}), \quad (46)$$

where \mathbf{m} denotes the variable vector that contains the elements of all K block-terms $\{\hat{\mathbf{G}}_k, \hat{\mathbf{A}}_k, \hat{\mathbf{s}}_k\}$ and $\boldsymbol{\mu}(\mathbf{m})$ denotes the vector of residuals, which is given by

$$\boldsymbol{\mu}(\mathbf{m}) \triangleq \text{vec} \left(\mathcal{Y} - \sum_{k=1}^K (\hat{\mathbf{G}}_k \hat{\mathbf{A}}_k^T) \circ \hat{\mathbf{s}}_k \right) \in \mathbb{C}^{MPT}. \quad (47)$$

Then, the Jacobian matrix at the point $\mathbf{m}^{(t)}$ can be computed by $\mathbf{J}^{(t)} = \frac{\partial \boldsymbol{\mu}(\mathbf{m}^{(t)})}{\partial \mathbf{m}^{(t)}}$, and the parameter vector can be updated iteratively using the Gauss-Newton or LM step as follows

$$\mathbf{m}^{(t+1)} = \mathbf{m}^{(t)} + \left((\mathbf{J}^{(t)})^H \mathbf{J}^{(t)} + \lambda^{(t+1)} \mathbf{I} \right)^{-1} (\mathbf{J}^{(t)})^H \mathbf{m}^{(t)}, \quad (48)$$

where $\lambda^{(t+1)}$ denotes the damping parameter at the $(t+1)$ -th iteration. Eq. (48) behaves as a Gauss-Newton update for a small value of $\lambda^{(t+1)}$, and approaches a LM update when $\lambda^{(t+1)}$ becomes large. Compared with the ALS algorithm, which updates one factor matrix at one time, the NLS algorithm performs a global optimization over all factors simultaneously, leading to faster convergence and improved reconstruction accuracy [29], [33].

To ensure fast and stable convergence of the NLS-based BTD algorithm, the initial factor matrices need to be elaborately designed. Below we discuss how to obtain the initialization factor matrices for the NLS-based algorithm. Based on the BTD representation (38), the mode-3 unfolding $\mathbf{Y}_{(3)} \in \mathbb{C}^{T \times MP}$ of \mathcal{Y} can be expressed as

$$\mathbf{Y}_{(3)} = \mathbf{S}_o [(\mathbf{G}_1 \odot \mathbf{A}_1) \mathbf{1}_{L_1} \cdots (\mathbf{G}_K \odot \mathbf{A}_K) \mathbf{1}_{L_k}]^T. \quad (49)$$

Since the pilot matrix \mathbf{S}_o is known *a priori* at the BS, we first removes the mixing effect of \mathbf{S}_o via a regularized pseudo-inverse operation, i.e., $\mathbf{X}_{(3)} = \mathbf{S}_o^\dagger \mathbf{Y}_{(3)}$, where $\mathbf{S}_o^\dagger = (\mathbf{S}_o^H \mathbf{S}_o + \epsilon \mathbf{I}_K)^{-1} \mathbf{S}_o^H$ with $\epsilon > 0$ being the regularization parameter. The k -th column of $\mathbf{X}_{(3)}(:, k)$ can be then reshaped into a $P \times M$ matrix, which provides a coarse approximation of $\mathbf{G}_k^T \mathbf{A}_k$, i.e.,

$$\mathbf{X}_k = \text{reshape}(\mathbf{X}_{(3)}(:, k), P, M) \approx \mathbf{G}_k^T \mathbf{A}_k \in \mathbb{C}^{P \times M}. \quad (50)$$

Then, the initial rank- L_k BTD factors $\mathbf{G}_k^{(0)}$ and $\mathbf{A}_k^{(0)}$ can be extracted using truncated singular value decomposition (SVD). Specifically, we have

$$\begin{aligned} \mathbf{X}_k &= \mathbf{U}_k \mathbf{\Lambda}_k \mathbf{V}_k, \\ \hat{\mathbf{G}}_k^{(0)} &= \mathbf{V}_k(:, 1:L_k) \mathbf{\Lambda}_k^{\frac{1}{2}} (1:L_k, 1:L_k), \\ \hat{\mathbf{A}}_k^{(0)} &= \mathbf{U}_k(:, 1:L_k) \mathbf{\Lambda}_k^{\frac{1}{2}} (1:L_k, 1:L_k), \end{aligned} \quad (51)$$

where $\mathbf{\Lambda}_k$ is a diagonal matrix with the singular values $\lambda_{k,i}$ being placed in a descending order on the diagonal, and the columns of \mathbf{U}_k and \mathbf{V}_k are the corresponding singular vectors.

After obtaining the initialization factor matrices, the NLS-based algorithm can be employed to iteratively refine their estimates. According to Theorem 2, the BTD is unique up to scaling and permutation ambiguities under some mild conditions, i.e.,

$$\begin{aligned} \hat{\mathbf{G}} &= \mathbf{G} \mathbf{\Lambda}_1 \mathbf{\Pi} + \mathbf{E}_1, \\ \hat{\mathbf{A}} &= \mathbf{A} \mathbf{\Lambda}_2 \mathbf{\Pi} + \mathbf{E}_2, \\ \hat{\mathbf{S}}_o &= \mathbf{S}_o \mathbf{\Lambda}_3 \mathbf{\Pi}_s + \mathbf{E}_3, \end{aligned} \quad (52)$$

where $\mathbf{G} = [\mathbf{G}_1 \cdots \mathbf{G}_K]$, $\mathbf{A} = [\mathbf{A}_1 \cdots \mathbf{A}_K]$, $\mathbf{\Lambda}_1 = \text{blkdiag}(\mathbf{\Lambda}_{1,1}, \dots, \mathbf{\Lambda}_{1,K})$ and $\mathbf{\Lambda}_2 = \text{blkdiag}(\mathbf{\Lambda}_{2,1}, \dots, \mathbf{\Lambda}_{2,K})$ are non-singular K -block diagonal matrices and $\mathbf{\Lambda}_3 = \text{diag}(\lambda_{3,1}, \dots, \lambda_{3,K})$ is a non-singular diagonal matrix, which satisfy $\lambda_{3,k} \mathbf{\Lambda}_{1,k} \mathbf{\Lambda}_{2,k}^T = \mathbf{I}_{L_k}, \forall k = 1, \dots, K$; $\mathbf{\Pi}$ is a K -block permutation matrix, $\mathbf{\Pi}_s$ is a permutation matrix, and both share the same permutation pattern; \mathbf{E}_1 , \mathbf{E}_2 and \mathbf{E}_3 denote the estimation errors of the BTD.

D. Channel Estimation

After obtaining the estimated factor matrices $(\hat{\mathbf{G}}, \hat{\mathbf{A}}, \hat{\mathbf{S}})$ via the NLS algorithm, we first estimate the permutation matrix $\mathbf{\Pi}_s$ to establish the correspondence between the recovered BTD components and the users. By exploiting the knowledge of the pilot sequences, this association can be efficiently determined using a correlation-based method, similar to that employed in the LoS-dominated scenarios. Specifically, $\mathbf{\Pi}_s$ is a $K \times K$ permutation matrix, and $\mathbf{\Pi}$ is a block-permutation

matrix consisting of $K \times K$ blocks. If the k -th column of \mathbf{S}_o is highly correlated with the k' -th column of $\hat{\mathbf{S}}_o$, then the (k', k) -th element of $\mathbf{\Pi}_s$ is set to 1, and the corresponding (k', k) -th block of $\mathbf{\Pi}$ is set to an identity matrix \mathbf{I}_{L_k} . Otherwise, the corresponding entry of $\mathbf{\Pi}_s$ is 0, and the corresponding block of $\mathbf{\Pi}$ is set to a all-zeros matrix. For instance, consider a 3×3 permutation matrix

$$\mathbf{\Pi}_s = \begin{bmatrix} 0 & 1 & 0 \\ 1 & 0 & 0 \\ 0 & 0 & 1 \end{bmatrix}. \quad (53)$$

Let $\mathbf{\Pi} \in \mathbb{R}^{8 \times 10}$ be a 3×3 block permutation matrix that follows the same permutation pattern, where the block sizes are 2, 3 and 4, respectively. Then, $\mathbf{\Pi}$ can be written as

$$\mathbf{\Pi} = \begin{bmatrix} \mathbf{0}_{2 \times 3} & \mathbf{I}_3 & \mathbf{0}_{2 \times 4} \\ \mathbf{I}_2 & \mathbf{0}_{3 \times 2} & \mathbf{0}_{3 \times 4} \\ \mathbf{0}_{4 \times 3} & \mathbf{0}_{4 \times 2} & \mathbf{I}_4 \end{bmatrix}. \quad (54)$$

After that, the permutation ambiguity for the estimated factor matrices can be removed. Thus, we have

$$\begin{aligned} \hat{\mathbf{G}} &= \hat{\mathbf{G}} \mathbf{\Pi}^T = \mathbf{G} \mathbf{\Lambda}_1 + \mathbf{E}_1, \\ \hat{\mathbf{A}} &= \hat{\mathbf{A}} \mathbf{\Pi}^T = \mathbf{A} \mathbf{\Lambda}_2 + \mathbf{E}_2, \\ \hat{\mathbf{S}}_o &= \hat{\mathbf{S}}_o \mathbf{\Pi}_s^T = \mathbf{S}_o \mathbf{\Lambda}_3 + \mathbf{E}_3. \end{aligned} \quad (55)$$

Similar to (27), the delay parameter τ_l associated with the l -th path component can be estimated via

$$\hat{\tau}_l = \arg \max_{\tau} \frac{|\mathbf{g}^H(\tau) \hat{\mathbf{g}}_l|}{\|\mathbf{g}(\tau)\|_2 \|\hat{\mathbf{g}}_l\|_2}. \quad (56)$$

For the multi-path scenario, the distance parameter cannot be simply obtained from $\{\hat{\tau}_l\}$. Note that the l -th column of $\hat{\mathbf{A}}$ is a scaled version of $\tilde{\mathbf{b}}(\theta_l, r_l) \triangleq \mathbf{W}^H \mathbf{b}(\theta_l, r_l)$. Thus, letting $\hat{\mathbf{a}}_l$ denote the l -th column of $\hat{\mathbf{A}}$, the angle-distance parameters can be jointly estimated by

$$\hat{\theta}_l, \hat{r}_l = \arg \max_{\theta, r} \frac{|\mathbf{b}^H(\theta, r) \mathbf{W} \hat{\mathbf{a}}_l|}{\|\mathbf{W}^H \mathbf{b}(\theta, r)\|_2 \|\hat{\mathbf{a}}_l\|_2}. \quad (57)$$

The search grid of the problem (57) can be obtained by constructing an overcomplete polar-domain codebook as that in [10]. As analyzed in [16], the correlation-based scheme in (56) and (57) is a maximum likelihood (ML) estimator, provided that the entries of the estimation error matrices \mathbf{E}_1 and \mathbf{E}_2 are i.i.d. complex Gaussian.

Next, we try to recover the path loss gains $\{\hat{\alpha}_l\}$. After obtaining $\{\hat{\tau}_l, \hat{\theta}_l, \hat{r}_l\}$, we can reconstruct

$$\begin{aligned} \tilde{\mathbf{G}} &= [\mathbf{g}(\hat{\tau}_1) \cdots \mathbf{g}(\hat{\tau}_L)], \\ \tilde{\mathbf{B}} &= \mathbf{W}^H [\mathbf{b}(\hat{\theta}_1, \hat{r}_1) \cdots \mathbf{b}(\hat{\theta}_L, \hat{r}_L)]. \end{aligned} \quad (58)$$

Ignoring the estimation error, the scaling ambiguity matrices can be estimated as $\mathbf{\Lambda}_1 = \tilde{\mathbf{G}}^\dagger \tilde{\mathbf{G}}$ and $\mathbf{\Lambda}_3 = \mathbf{S}_o^\dagger \hat{\mathbf{S}}_o$. Moreover, since $\lambda_{3,k} \mathbf{\Lambda}_{1,k} \mathbf{\Lambda}_{2,k}^T = \mathbf{I}_{L_k}, \forall k = 1, \dots, K$, we have

$$\mathbf{\Lambda}_2^\dagger = \text{blkdiag}(\lambda_{3,1} \mathbf{\Lambda}_{1,1}^T, \dots, \lambda_{3,K} \mathbf{\Lambda}_{1,K}^T). \quad (59)$$

Ideally we should have $\hat{\mathbf{A}} = \tilde{\mathbf{B}} \mathbf{D}_\alpha \mathbf{\Lambda}_2$, where $\mathbf{D}_\alpha \triangleq \text{diag}(\alpha_1, \dots, \alpha_L)$. Hence, \mathbf{D}_α can be estimated as

$$\hat{\mathbf{D}}_\alpha = \text{diag}(\tilde{\mathbf{B}}^\dagger \hat{\mathbf{A}} \mathbf{\Lambda}_2^\dagger). \quad (60)$$

Finally, the channels $\{\mathbf{h}_{p,k}\}$ can be reconstructed by the estimated parameters $\{\hat{\tau}_l, \hat{\theta}_l, \hat{r}_l, \hat{\alpha}_l\}$ according to (1).

VI. SIMULATION RESULTS

In this section, we present simulation results to illustrate the performance of the proposed CPD/BTD-based near-field channel estimation and sensing method. For the LoS scenario, since the dominant LoS path provides reliable geometric information, the recovered channel parameters allow not only accurate channel estimation but also precise user localization. Therefore, both channel estimation performance and localization accuracy are evaluated. For the NLoS scenario, we only focus on evaluating the channel estimation performance of the proposed method.

In our simulations, the signal-to-noise ratio (SNR) is defined as

$$\text{SNR} \triangleq \|\mathcal{Y} - \mathcal{N}\|_F^2 / \|\mathcal{N}\|_F^2. \quad (61)$$

We also derive the Cramér–Rao bounds (CRBs) for both the channel parameters and the user positions, which serve as a theoretical lower bound for evaluating the estimation accuracy of channel parameters and user locations. The detailed derivations of the CRB are provided in Appendix. The normalized mean square error (NMSE) is used to quantify the channel estimation performance, which is defined as

$$\text{NMSE} \triangleq \frac{\sum_{p=1}^P \sum_{k=1}^K \|\mathbf{h}_{p,k} - \hat{\mathbf{h}}_{p,k}\|_F^2}{\sum_{p=1}^P \sum_{k=1}^K \|\mathbf{h}_{p,k}\|_F^2}. \quad (62)$$

The pilot symbol matrix \mathbf{S}_o is chosen from the codebook of Grassmannian beamforming [34] for $T = 2$. While for $3 \leq T < 8$, \mathbf{S}_o can be calculated by the algorithm proposed in [35]. When $T = 8$, \mathbf{S}_o is simply chosen as a DFT matrix.

A. MMV-Based Channel Estimation Benchmarks

Owing to the sparse scattering nature of mmWave/THz channel, the multi-user channel estimation considered in this paper can also be reformulated as a multiple-measurement-vector (MMV) compressed sensing problem. Taking the mode-1 unfolding of \mathcal{Y} in (9), we have

$$\begin{aligned} \mathbf{Y}_{(1)}^T &= (\mathbf{S} \odot \mathbf{A})\mathbf{G}^T + \mathbf{N}_{(1)}^T \\ &= (\mathbf{S} \otimes \mathbf{W}^H \bar{\mathbf{B}})^T (\mathbf{O} \otimes \mathbf{X}_B) \mathbf{D}_\alpha \mathbf{G}^T + \mathbf{N}_{(1)}^T \end{aligned} \quad (63)$$

where $\mathbf{Y}_{(1)}$ and $\mathbf{N}_{(1)}$ are the mode-1 unfolding of \mathcal{Y} and \mathcal{N} , respectively; $\bar{\mathbf{B}} \in \mathbb{C}^{N \times Q}$ is the near-field polar-domain codebook [10]; $\mathbf{X}_B \in \mathbb{C}^{Q \times P}$ is a sparse matrix whose different columns exhibit the same sparsity pattern. Define

$$\begin{aligned} \Phi &\triangleq \mathbf{S} \otimes \mathbf{W}^H \bar{\mathbf{B}}, \\ \mathbf{X} &\triangleq (\mathbf{O} \otimes \mathbf{X}_B) \mathbf{D}_\alpha \mathbf{G}^T \end{aligned} \quad (64)$$

It is obvious that \mathbf{X} is obtained by augmenting \mathbf{X}_B with zero rows and thus its columns also exhibit the common sparsity pattern. Consequently, the mode-1 unfolding of \mathcal{Y} can be re-written as

$$\mathbf{Y}_{(1)}^T = \Phi \mathbf{X} + \mathbf{N}_{(1)}^T. \quad (65)$$

The above problem can be solved by the simultaneous orthogonal matching pursuit (SOMP) [10] and the simultaneous iterative gridless weighted (SIGW) [10] algorithms, which are adopted as the benchmarks in our simulations.

B. LoS Scenarios (THz Bands)

We first consider an ELAA THz systems where the propagation is dominated by a strong LoS component due to its limited diffraction and severe path loss/molecular absorption. The carrier frequency is set to $f_c = 100$ GHz with a bandwidth of $B = 0.1$ GHz. In addition, the number of OFDM subcarriers is set to $P = 64$. The BS is equipped with $N = 256$ antennas and $M = 32$ RF chains. The corresponding Rayleigh distance is calculated as $d_R = 97.5$ meters. The gain of the LoS path is generated as [3]:

$$\alpha_{\text{LoS}} = \frac{c}{4\pi f d} \exp\left(-\frac{1}{2}K(f)d\right) \exp(-j2\pi f\tau) \quad (66)$$

where f and d denote the frequency and the propagation distance, respectively. The time delay of the LoS path is given by $\tau = (d/c)$. The molecular absorption coefficient, $K(f)$, characterizes the frequency-selective attenuation caused by molecular energy conversion in the propagation medium [3] and is set to 0.01 in our experiment.

We consider $K = 8$ users located in the near-field region of the BS. For each user, the angle θ_k and the distance r_k from the reference antenna to each user are randomly drawn from $\mathcal{U}(20 \text{ m}, 80 \text{ m})$ and $\mathcal{U}(-60^\circ, 60^\circ)$, respectively. The corresponding time-delay is then computed as $\tau_k = r_k/c$.

Note that after the factor matrices are estimated, there are two different strategies in estimating the angle and distance parameters in the LoS scenarios. The first approach is to perform a joint estimation of the distance and the angle according to (30) based on the estimated factor matrix $\hat{\mathbf{A}}$. This approach involves a correlation-based search in a near-field codebook constructed by jointly sampling over the two-dimensional angle-range domain. The second approach, instead, extracts the distance information from the estimated delay parameter. Since we have $\hat{r}_k = \hat{\tau}_k c$ for the LoS scenario, the distance information can be readily obtained after the delay parameters are estimated from the recovered factor matrix $\hat{\mathbf{G}}$. After the distance \hat{r}_k is estimated, the angle parameter θ_k can be estimated via (31) with the distance treated as known. In fact, the latter approach usually yields a more accurate estimate of the distance parameter. This is because the factor matrix \mathbf{G} has a Vandermonde structure which provides a better resolvability for different distances, while columns in the factor matrix $\hat{\mathbf{A}}$ are constructed from near-field steering vectors that are highly correlated even for different distance parameters. In our simulations, the first approach is referred to as “CPD-based” while the latter approach is specifically termed as “CPD-based (delay-aided)”.

1) *Evaluation of Channel Parameter Estimation Performance:* In Fig. 2, we plot the mean square errors (MSEs) of the estimated channel parameters $\{\tau, \theta, r\}$ as a function of the SNR, where we set $T = 4$, $P = 64$ and $M = 32$. It can be observed that the MSEs attained by our proposed CPD-based method gradually approach the corresponding CRBs as

the SNR increases. On the other hand, as explained earlier, the “CPD-based (delay-aided)” method can achieve a much more accurate estimate of the distance parameter by utilizing the delay information. Note that since the “CPD-based (delay-aided)” method leverages the relation between time-delay and distance, which introduces extra prior knowledge to the estimation problem, it is no wonder that “CPD-based (delay-aided)” can achieve a lower MSE of the distance estimate than the theoretical CRB.

2) *Evaluation of User Localization Performance*: As shown in Appendix, the CRB for user location is derived based on the estimated τ and θ . Therefore, the user location CRB characterizes the fundamental limit of the “CPD-based (delay-aided)” method, whose MSE is clearly lower-bounded by it. In Fig. 3(a), it can be observed that the proposed “CPD-based (delay-aided)” method is capable of achieving a millimeter-level localization accuracy when SNR is above 5 dB. In contrast, the MSE of the “CPD-based” method that directly estimates the angle-distance pairs from the recovered factor matrix $\hat{\mathbf{A}}$ are far from the CRB. The primary reason, as discussed before, is that the phase of a near-field spherical wavefront varies slowly with distance, making the coherence of near-field steering vectors less sensitive to the variation of distance. As a result, it becomes highly challenging to obtain a high-precision estimate of the distance \mathbf{r} simply from the factor matrix $\hat{\mathbf{A}}$, which in turn affects the user localization performance.

Fig. 3(b) illustrates the MSEs of estimated user locations versus the number of RF chains. We see that the MSE of the “CPD-based (delay-aided)” method converges quickly to the CRB, demonstrating that the proposed method can achieve high-accuracy user localization performance even with a relatively small number of RF chains.

Fig. 3(c) depicts the MSEs as a function of the length of the pilot sequence. It can be observed that the proposed “CPD-based (delay-aided)” method can achieve superior localization performance even when the number of pilot symbols is much less than the number of users. This result demonstrates the potential of the proposed method in substantially reducing the training overhead.

3) *Evaluation of Channel Estimation Performance*: Fig. 4 plots the NMSE performance of respective algorithms. It can be observed that both the “CPD-based” and “CPD-based (delay-aided)” methods present a significant performance improvement over the compressed sensing (CS)-based baselines. This is attributed to the fact that the proposed methods effectively explore the intrinsic multi-dimensional low-rank structure of near-field OFDM channels. The “CPD-based (delay-aided)” method slightly outperforms the “CPD-based” method owing to its more accurate estimation of the distance parameters.

C. NLoS Scenarios

To demonstrate the effectiveness of our proposed method for more general settings, we consider NLoS scenarios where the LoS path is blocked between each user and the BS, and there exist multiple NLoS paths from the user to the BS. In

our simulations, the carrier frequency is set to $f_c = 30$ GHz with a bandwidth of $B = 0.1$ GHz. The BS is equipped with $N = 128$ antennas and $M = 64$ RF chains. Accordingly, the Rayleigh distance is given by $d_R = 80.6$ m. The number of NLoS paths between the BS and each user is randomly selected from $\{1, 2\}$ and the complex path gain of each NLoS path follows $\alpha_{k,l} \sim \mathcal{CN}(0, 10^{-0.1(\kappa+\mu)})$, where $\kappa = a + 10b \log_{10}(d) + \epsilon$, with d being the distance between the BS and the k -th user, $\mu = 7$ dB denoting the Rician factor and $\epsilon \in \mathcal{CN}(0, \sigma_\epsilon^2)$ [36]. Here, we set $a = 61.4$, $b = 2$ and $\sigma_\epsilon = 5.8$ dB as suggested in [36]. The time delay associated with the (k, l) -th path is given by $\tau_{k,l} = \tilde{\tau}_{k,l} + r_{k,l}/c$, where $\tilde{\tau}_{k,l}$ represents the propagation delay from the k -th user to the scatterer of the (k, l) -th path and is randomly chosen from $[0, 2 \times 10^{-9}]$ seconds(s). Unless otherwise specified, the other simulation parameters are set the same as that in LoS scenarios.

Fig. 5 illustrates the NMSE performance of our proposed BTD-based method and the CS-based MMV methods, where we set $T = 4$ and $M = 64$. It can be observed that, our proposed BTD-based method outperforms the SOMP method by a big margin across different SNR settings. Compared with the SIGW method, a significant performance improvement can be observed at the low-SNR regime. As shown in Fig. 5(c), our proposed method has a performance similar to the compressed sensing-based method when $T = 2$. This is because the BTD model has a weak uniqueness guarantee in this case. When the user channels exhibit relatively high correlation, the resulting BTD suffers severe decomposition ambiguity, which degrades the accuracy of the subsequent channel estimation.

VII. CONCLUSION

In this paper, we developed a tensor decomposition-based method for integrated near-field multi-user channel estimation and user localization in ELAA THz systems. To improve scalability with an increasing number of users, we consider a non-orthogonal pilot transmission scheme where the pilot length is smaller than the number of users. By exploring the intrinsic multi-dimensional low-rank structure of near-field channels, the received signal is modeled as a third-order tensor that admits a CPD representation in LoS scenarios and a BTD representation in the general multi-path environments. These tensor structures enable effective decoupling of path components across different users and facilitate accurate channel estimation and user localization. Our uniqueness analysis further provides a theoretical guarantee for reliable joint estimation under the non-orthogonal pilot transmission, showing that the multi-user channel parameters can be jointly and uniquely recovered as long as the pilot length satisfies $T \geq 2$. Through extensive simulations, we validated the superiority of the proposed methods compared to the CS-based channel estimation methods.

APPENDIX

Consider the $P \times M \times T$ observation tensor \mathcal{Y} in (9)

$$\mathcal{Y} = \sum_{l=1}^L \alpha_l \mathbf{g}(\tau_l) \circ (\mathbf{W}^H \mathbf{b}(\theta_l, r_l)) \circ \tilde{\mathbf{s}}_l + \mathcal{N}, \quad (67)$$

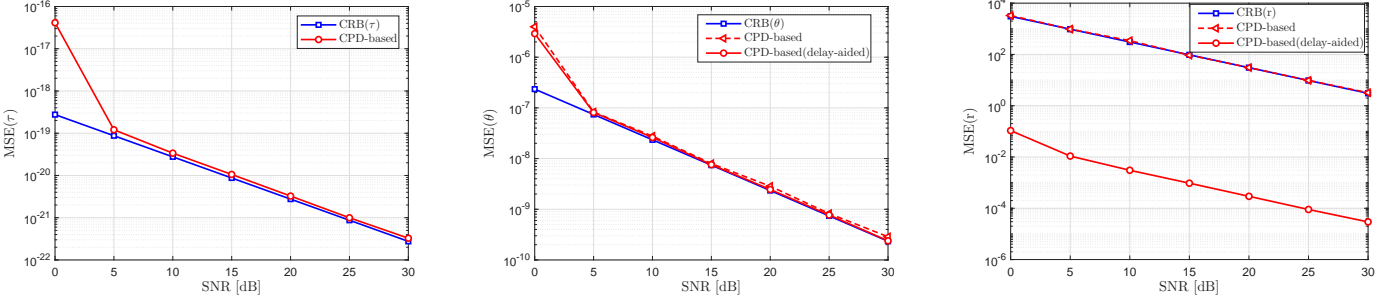


Fig. 2: MSEs/CRBs for channel parameter estimation versus SNR (dB), where $T = 4$ and $M = 32$.

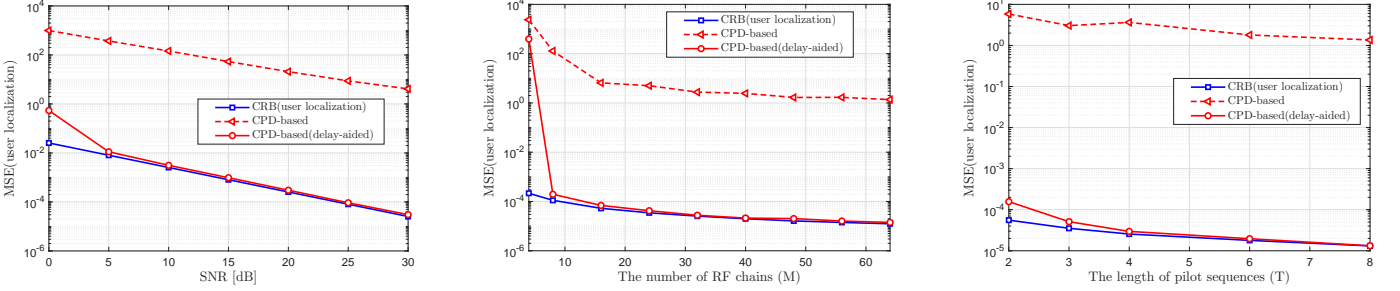


Fig. 3: (a) MSE/CRB for user localization versus SNR (dB), where $T = 4$ and $M = 32$; (b) MSE/CRB for user localization versus the number of RF chains (M), where $T = 4$ and SNR = 30 dB; (c) MSE/CRB for user localization versus the pilot sequences (T), where $M = 32$ and SNR = 30 dB.

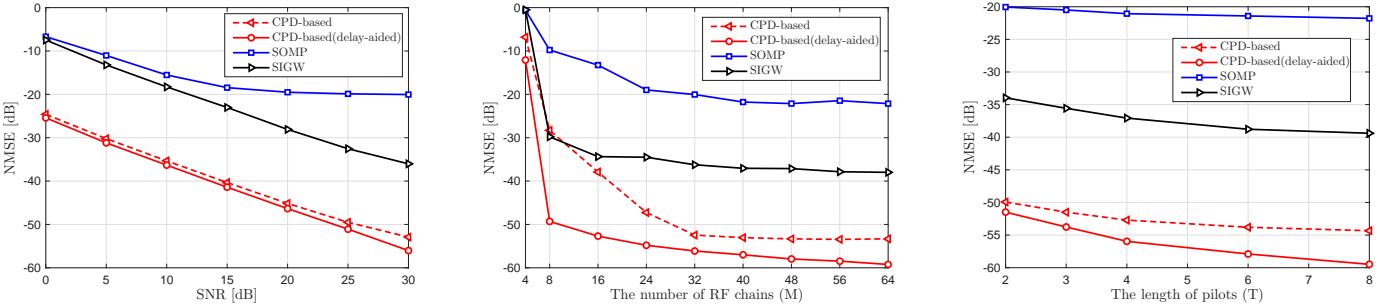


Fig. 4: (a) NMSE versus SNR (dB), where $T = 4$ and $M = 32$; (b) NMSE versus the number of RF chains (M), where $T = 4$ and SNR = 30 dB; (c) NMSE versus the length of pilot sequences (T), where $M = 32$ and SNR = 30 dB.

where $\mathcal{N}(m, p, t) \sim \mathcal{CN}(0, \sigma^2)$, $\{\alpha_l, \tau_l, \theta_l, r_l\}$ are the unknown channel parameters to be estimated. Let $\xi \triangleq [\theta^T \ r^T \ \tau^T \ \alpha_R^T \ \alpha_I^T]^T \in \mathbb{R}^{5K}$ denote the parameter vector, where

$$\begin{aligned} \theta &\triangleq [\theta_1 \ \dots \ \theta_K]^T \in \mathbb{R}^K, \\ \tau &\triangleq [\tau_1 \ \dots \ \tau_K]^T \in \mathbb{R}^K, \\ r &\triangleq [r_1 \ \dots \ r_K]^T \in \mathbb{R}^K, \\ \alpha_R &\triangleq [\text{Re}\{\alpha_1\} \ \dots \ \text{Re}\{\alpha_K\}]^T \in \mathbb{R}^K, \\ \alpha_I &\triangleq [\text{Im}\{\alpha_1\} \ \dots \ \text{Im}\{\alpha_K\}]^T \in \mathbb{R}^K. \end{aligned} \quad (68)$$

By stacking the tensor entries in (67) into a vector form, the received signal can be re-written as

$$\mathbf{y}_v = \boldsymbol{\mu}(\xi) + \mathbf{n}_v \in \mathbb{C}^{MPT}, \quad (69)$$

where $\mathbf{y}_v \triangleq \text{vec}(\mathcal{Y})$, $\mathbf{n}_v \triangleq \text{vec}(\mathcal{N}) \in \mathbb{C}^{MPT}$ and

$$\boldsymbol{\mu}(\xi) \triangleq \sum_{l=1}^L \alpha_l (\tilde{\mathbf{s}}_l \otimes (\mathbf{W}^H \mathbf{b}(\theta_l, r_l)) \otimes \mathbf{g}(\tau_l)) \in \mathbb{C}^{MPT}. \quad (70)$$

Thus, the log-likelihood function of ξ can be expressed as

$$L(\xi) = -MPT \ln(\pi\sigma^2) - \frac{1}{\sigma^2} \|\mathbf{y}_v - \boldsymbol{\mu}(\xi)\|_F^2. \quad (71)$$

A. Derivation of CRBs for Channel Parameters

The Fisher Information matrix (FIM) for estimating the vector ξ is given by

$$\begin{aligned} \mathbf{F}_\xi &\triangleq \mathbb{E} \left\{ \left(\frac{\partial L(\xi)}{\partial \xi} \right)^H \left(\frac{\partial L(\xi)}{\partial \xi} \right) \right\} \\ &= \frac{2}{\sigma^2} \text{Re} \left\{ \left(\frac{\partial \boldsymbol{\mu}(\xi)}{\partial \xi} \right)^H \left(\frac{\partial \boldsymbol{\mu}(\xi)}{\partial \xi} \right) \right\}, \end{aligned} \quad (72)$$

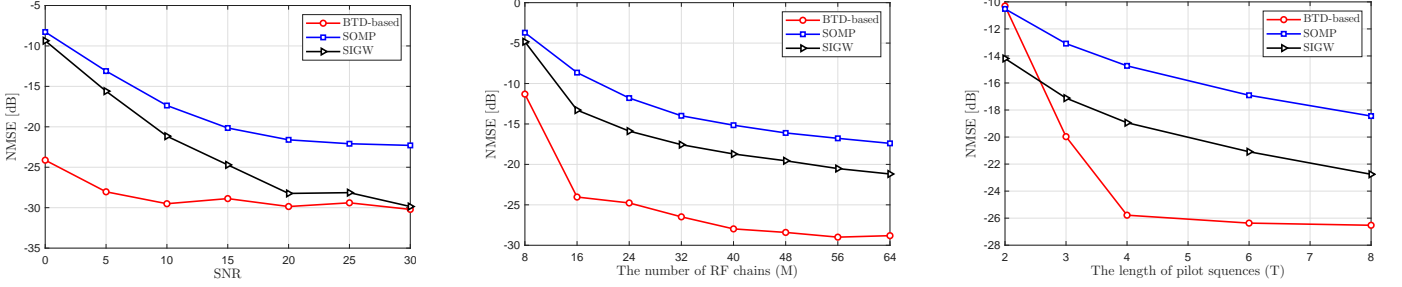


Fig. 5: (a) NMSE versus SNR (dB), where $T = 4$ and $M = 64$; (b) NMSE versus the number of RF chains (M), where $T = 4$ and SNR = 10 dB; (c) NMSE versus the length of pilot sequences (T), where $M = 64$ and SNR = 10 dB.

where $\frac{\partial \mu(\xi)}{\partial \xi}$ denotes the Jacobian matrix collecting the first-order partial derivatives of $\mu(\xi)$ w.r.t. each parameter, i.e.,

$$\begin{aligned} \frac{\partial \mu(\xi)}{\partial \xi} &\triangleq \begin{bmatrix} \frac{\partial \mu(\xi)}{\partial \tau} & \frac{\partial \mu(\xi)}{\partial \theta} & \frac{\partial \mu(\xi)}{\partial r} & \frac{\partial \mu(\xi)}{\partial \alpha_R} & \frac{\partial \mu(\xi)}{\partial \alpha_I} \end{bmatrix} \in \mathbb{C}^{MPT \times 5K}, \\ \frac{\partial \mu(\xi)}{\partial \mathbf{a}} &\triangleq \begin{bmatrix} \frac{\partial \mu(\xi)}{\partial a_1} & \dots & \frac{\partial \mu(\xi)}{\partial a_K} \end{bmatrix} \in \mathbb{C}^{MPT \times K}, \\ \mathbf{a} &\in \{\tau, \theta, r, \alpha_R, \alpha_I\}. \end{aligned} \quad (73)$$

Specifically, we have

$$\begin{aligned} \frac{\partial \mu(\xi)}{\partial \tau_l} &= \alpha_l \tilde{\mathbf{s}}_l \otimes (\mathbf{W}^H \mathbf{b}(\theta_l, r_l)) \otimes \frac{\partial \mathbf{g}(\tau_l)}{\partial \tau_l} \\ \frac{\partial \mu(\xi)}{\partial \theta_l} &= \alpha_l \tilde{\mathbf{s}}_l \otimes \left(\mathbf{W}^H \frac{\partial \mathbf{b}(\theta_l, r_l)}{\partial \theta_l} \right) \otimes \mathbf{g}(\tau_l), \\ \frac{\partial \mu(\xi)}{\partial r_l} &= \alpha_l \tilde{\mathbf{s}}_l \otimes \left(\mathbf{W}^H \frac{\partial \mathbf{b}(\theta_l, r_l)}{\partial r_l} \right) \otimes \mathbf{g}(\tau_l), \\ \frac{\partial \mu(\xi)}{\partial \text{Re}\{\alpha_l\}} &= \tilde{\mathbf{s}}_l \otimes \left(\mathbf{W}^H \mathbf{b}(\theta_l, r_l) \right) \otimes \mathbf{g}(\tau_l), \\ \frac{\partial \mu(\xi)}{\partial \text{Re}\{\alpha_l\}} &= j \tilde{\mathbf{s}}_l \otimes (\mathbf{W}^H \mathbf{b}(\theta_l, r_l)) \otimes \mathbf{g}(\tau_l), \end{aligned} \quad (74)$$

where the derivative of the steering vectors are given by

$$\begin{aligned} \frac{\partial \mathbf{g}(\tau_l)}{\partial \tau_l} &= -j 2\pi \text{diag}(f_1, \dots, f_P) \mathbf{g}(\tau_l), \\ \left[\frac{\partial \mathbf{b}(\theta_l, r_l)}{\partial \theta_l} \right]_n &= j \frac{2\pi}{\lambda} \left(\frac{r_l(n-1)d \cos \theta_l}{r_l^{(n)}} \right) \mathbf{b}_n, \quad \forall n, \\ \left[\frac{\partial \mathbf{b}(\theta_l, r_l)}{\partial r_l} \right]_n &= -j \frac{2\pi}{\lambda} \left(\frac{r_l - (n-1)d \sin \theta_l}{r_l^{(n)}} - 1 \right) \mathbf{b}_n, \quad \forall n, \end{aligned} \quad (75)$$

in which $\left[\frac{\partial \mathbf{b}(\theta_l, r_l)}{\partial \theta_l} \right]_n$, $\left[\frac{\partial \mathbf{b}(\theta_l, r_l)}{\partial r_l} \right]_n$ and \mathbf{b}_n represent the n -th element of $\frac{\partial \mathbf{b}(\theta_l, r_l)}{\partial \theta_l}$, $\frac{\partial \mathbf{b}(\theta_l, r_l)}{\partial r_l}$ and $\mathbf{b}(\theta_l, r_l)$, respectively.

Then, the CRB for estimation error of $\mathbf{a} \in \{\tau, \theta, r, \alpha_R, \alpha_I\}$ can be expressed as

$$\text{MSE}(\mathbf{a}) = \|\hat{\mathbf{a}} - \mathbf{a}\|_F^2 \geq \text{CRB}(\mathbf{a}) = \text{tr} \left(\left[\mathbf{F}_\xi^{-1} \right]_{\mathcal{I}_a, \mathcal{I}_a} \right), \quad (76)$$

where \mathcal{I}_a is the index associated with the parameter \mathbf{a} . For example, $\mathcal{I}_\theta = [1, \dots, K]$.

B. Derivation of CRBs for User Localization

After obtaining the channel parameters $\{\hat{\theta}_k, \hat{\tau}_k\}_{k=1}^K$, the position of the k -th user can be calculated as

$$\mathbf{p}_k \triangleq \left[c \hat{\tau}_k \cos \hat{\theta}_k, c \hat{\tau}_k \sin \hat{\theta}_k \right]^T. \quad (77)$$

Let $\mathbf{p} \triangleq [\mathbf{p}_1 \dots \mathbf{p}_K]^T \in \mathbb{R}^{2K}$. The FIM for user localization can be obtained based on the FIM in (72), which is given by

$$\mathbf{F}_p = \mathbf{J}_{p/\xi} \mathbf{F}_\xi \nabla_{\mathbf{p}_k} \mathbf{J}_{p/\xi}^T, \quad (78)$$

where $\mathbf{J}_{p/\xi}$ denotes the partial derivative matrix w.r.t. \mathbf{p} , whose size is $2K \times 5K$, i.e.,

$$\mathbf{J}_{p/\xi} \triangleq \left[\frac{\partial \theta^T}{\partial \mathbf{p}} \frac{\partial \tau^T}{\partial \mathbf{p}} \frac{\partial r^T}{\partial \mathbf{p}} \frac{\partial \alpha_R^T}{\partial \mathbf{p}} \frac{\partial \alpha_I^T}{\partial \mathbf{p}} \right]^T \in \mathbb{C}^{5K \times 2K}, \quad (79)$$

where

$$\begin{aligned} \frac{\partial \mathbf{a}^T}{\partial \mathbf{p}} &\triangleq \left[\frac{\partial a_1}{\partial \mathbf{p}} \dots \frac{\partial a_K}{\partial \mathbf{p}} \right]^T \in \mathbb{C}^{K \times 2K}, \mathbf{a} \in \{\tau, \theta, r, \alpha_R, \alpha_I\}, \\ \frac{\partial a_k}{\partial \mathbf{p}} &= \left[\frac{\partial a_k}{\partial p_1} \dots \frac{\partial a_k}{\partial p_K} \right] \in \mathbb{C}^{2K}, \forall k = 1, \dots, K. \end{aligned} \quad (80)$$

Specifically, we have

$$\begin{aligned} \frac{\partial \tau_k}{\partial \mathbf{p}_{k'}} &= \begin{cases} \mathbf{0}_2, & k \neq k', \\ \left[\frac{\partial \tau_k}{\partial p_{k,1}}, \frac{\partial \tau_k}{\partial p_{k,2}} \right]^T, & k = k', \end{cases} \\ \frac{\partial \theta_k}{\partial \mathbf{p}_{k'}} &= \begin{cases} \mathbf{0}_2, & k \neq k', \\ \left[\frac{\partial \theta_k}{\partial p_{k,1}}, \frac{\partial \theta_k}{\partial p_{k,2}} \right]^T, & k = k', \end{cases} \\ \frac{\partial r_k}{\partial \mathbf{p}_{k'}} &= \mathbf{0}_2, \forall k, k' = 1, \dots, K, \\ \frac{\partial \text{Re}\{\alpha_k\}}{\partial \mathbf{p}_{k'}} &= \mathbf{0}_2, \forall k, k' = 1, \dots, K, \\ \frac{\partial \text{Im}\{\alpha_k\}}{\partial \mathbf{p}_{k'}} &= \mathbf{0}_2, \forall k, k' = 1, \dots, K. \end{aligned} \quad (81)$$

To compute $\left\{ \frac{\partial \tau_k}{\partial p_{k,i}}, \frac{\partial \theta_k}{\partial p_{k,i}} \right\}$, $i = 1, 2$, we can first compute

$$\frac{\partial (p_{k,1}, p_{k,2})}{\partial (\tau_k, \theta_k)} = \begin{bmatrix} c \cos \theta_k & -c \tau_k \sin \theta_k \\ c \sin \theta_k & c \tau_k \cos \theta_k \end{bmatrix}. \quad (82)$$

Consequently, it can be derived that

$$\frac{\partial (\tau_k, \theta_k)}{\partial (p_{k,1}, p_{k,2})} = \left[\frac{\partial (p_{k,1}, p_{k,2})}{\partial (\tau_k, \theta_k)} \right]^{-1} = \begin{bmatrix} \frac{\cos \theta_k}{c} & \frac{\sin \theta_k}{c \tau_k} \\ \frac{-\sin \theta_k}{c \tau_k} & \frac{\cos \theta_k}{c \tau_k} \end{bmatrix}. \quad (83)$$

Finally, the CRBs for user localization is given by

$$\text{MSE}(\mathbf{p}) = \|\mathbf{p} - \hat{\mathbf{p}}\|_F^2 \geq \text{CRB}(\mathbf{p}) = \text{tr}(\mathbf{F}_p^{-1}). \quad (84)$$

REFERENCES

- [1] M. Cui, Z. Wu, Y. Lu, X. Wei, and L. Dai, "Near-field MIMO communications for 6G: Fundamentals, challenges, potentials, and future directions," *IEEE Commun. Mag.*, vol. 61, no. 1, pp. 40–46, Jan. 2023.
- [2] Z. Wang, J. Zhang, H. Du, D. Niyato, S. Cui, B. Ai, M. Debbah, K. B. Letaief, and H. V. Poor, "A tutorial on extremely large-scale MIMO for 6G: Fundamentals, signal processing, and applications," *IEEE Commun. Surveys Tuts.*, vol. 6, no. 3, pp. 1560–1605, 3rd Quart. 2024.
- [3] B. Ning, Z. Tian, W. Mei, Z. Chen, C. Han, S. Li, J. Yuan, and R. Zhang, "Beamforming technologies for ultra-massive MIMO in terahertz communications," *IEEE Open J. Commun. Soc.*, vol. 4, pp. 614–658, 2023.
- [4] H. Lu and Y. Zeng, "Near-field modeling and performance analysis for multi-user extremely large-scale MIMO communication," *IEEE Commun. Lett.*, vol. 26, no. 2, pp. 277–281, Feb. 2022.
- [5] Z. Zhou, X. Gao, J. Fang, and Z. Chen, "Spherical wave channel and analysis for large linear array in LoS conditions," in *Proc. IEEE Globecom Workshops (GC Wkshps)*, Dec. 2015, pp. 1–6.
- [6] J. Cong, C. You, J. Li, L. Chen, B. Zheng, Y. Liu, W. Wu, Y. Gong, S. Jin, and R. Zhang, "Near-field integrated sensing and communication: Opportunities and challenges," *IEEE Wireless Commun.*, vol. 31, no. 6, pp. 162–169, Dec. 2024.
- [7] F. Zhang, T. Mao, M. Li, M. Hua, J. Chen, C. Masouros, and Z. Wang, "Near-field ISAC for the wireless systems," *IEEE Network*, vol. 39, no. 6, pp. 54–61, Nov. 2025.
- [8] Z. Wei, H. Qu, Y. Wang, X. Yuan, H. Wu, Y. Du, K. Han, N. Zhang, and Z. Feng, "Integrated sensing and communication signals toward 5G-A and 6G: A survey," *IEEE Internet Things J.*, vol. 10, no. 13, pp. 11068–11092, Jul. 2023.
- [9] F. Liu, Y. Cui, C. Masouros, J. Xu, T. X. Han, Y. C. Eldar, and S. Buzzi, "Integrated sensing and communications: Toward dual-functional wireless networks for 6G and beyond," *IEEE J. Sel. Areas Commun.*, vol. 40, no. 6, pp. 1728–1767, Jun. 2022.
- [10] M. Cui and L. Dai, "Channel estimation for extremely large-scale MIMO: Far-field or near-field?" *IEEE Trans. Commun.*, vol. 70, no. 4, pp. 2663–2677, 2022.
- [11] S. Yue, S. Zeng, L. Liu, Y. C. Eldar, and B. Di, "Hybrid near-far field channel estimation for holographic MIMO communications," *IEEE Trans. Wireless Commun.*, vol. 23, no. 11, pp. 15 798–15 813, Nov. 2024.
- [12] S. Yang, C. Xie, W. Lyu, B. Ning, Z. Zhang, and C. Yuen, "Near-field channel estimation for extremely large-scale reconfigurable intelligent surface (XL-RIS)-aided wideband mmwave systems," *IEEE J. Sel. Areas Commun.*, vol. 42, no. 6, pp. 1567–1582, Jun. 2024.
- [13] J. N. Pisharody, A. Rajoriya, and R. Budhiraja, "Near-field channel estimation for XL-MIMO systems using variational bayesian learning," *IEEE Trans. Wireless Commun.*, vol. 23, no. 9, pp. 10 740–10 756, Sep. 2024.
- [14] H. Wang, J. Fang, H. Duan, H. Li, and L. Li, "Near/far-field channel estimation for terahertz systems with ELAAs: A block-sparsity-aware approach," *IEEE Trans. Commun.*, early access, Dec. 29, 2025, doi: [10.1109/TCOMM.2025.3648970](https://doi.org/10.1109/TCOMM.2025.3648970).
- [15] Z. Zhou, J. Fang, L. Yang, H. Li, Z. Chen, and S. Li, "Channel estimation for millimeter-wave multiuser MIMO systems via PARAFAC decomposition," *IEEE Trans. Wireless Commun.*, vol. 15, no. 11, pp. 7501–7516, 2016.
- [16] Z. Zhou, J. Fang, L. Yang, H. Li, Z. Chen, and R. S. Blum, "Low-rank tensor decomposition-aided channel estimation for millimeter wave MIMO-OFDM systems," *IEEE J. Sel. Areas Commun.*, vol. 35, no. 7, pp. 1524–1538, Jul. 2017.
- [17] S. Cheng, L. You, Z. Jin, L. Cheng, and X. Gao, "Tensor-based channel estimation for near-field millimeter wave XL-MIMO systems," *IEEE Wireless Commun. Lett.*, vol. 14, no. 7, pp. 1909–1913, Jul. 2025.
- [18] Y.-D. Huang and M. Barkat, "Near-field multiple source localization by passive sensor array," *IEEE Trans. Antennas Propag.*, vol. 39, no. 7, pp. 968–975, Jul. 1991.
- [19] W. Zhi and M. Y.-W. Chia, "Near-field source localization via symmetric subarrays," in *Proc. IEEE Int. Conf. Acoust. Speech and Signal Process. (ICASSP)*, vol. 2, 2007, pp. 1121–1124.
- [20] Ramezani, Parisa, TuğçeDemir, Özlem, and Björnson, Emil, *Localization in Massive MIMO Networks: From Far Field to Near Field*, 2025, pp. 123–150.
- [21] B. Teng, X. Yuan, R. Wang, Y.-C. Liang, and X. Huang, "Near-field multiuser localization based on extremely large antenna array with limited RF chains," *IEEE Trans. Wireless Commun.*, vol. 24, no. 12, pp. 10 211–10 226, Dec. 2025.
- [22] L. Qiao, A. Liao, Z. Li, H. Wang, Z. Gao, X. Gao, Y. Su, P. Xiao, L. You, and D. W. K. Ng, "Sensing user's activity, channel, and location with near-field extra-large-scale MIMO," *IEEE Trans. Commun.*, vol. 72, no. 2, pp. 890–906, Feb. 2024.
- [23] Z. Lu, Y. Han, S. Jin, and M. Matthaiou, "Near-field localization and channel reconstruction for ELAA systems," *IEEE Trans. Wireless Commun.*, vol. 23, no. 7, pp. 6938–6953, Jul. 2024.
- [24] L. Jiang, J. Guan, J. Du, W. Jiang, and Y. Cheng, "Near-field channel parameter estimation and localization for mmwave massive MIMO-OFDM ISAC systems via tensor analysis," *Sensors (Basel, Switzerland)*, vol. 25, no. 16, p. 5050, Aug. 2025.
- [25] B. Ning, Z. Chen, W. Chen, Y. Du, and J. Fang, "Terahertz multi-user massive MIMO with intelligent reflecting surface: Beam training and hybrid beamforming," *IEEE Trans. Veh. Technol.*, vol. 70, no. 2, pp. 1376–1393, Feb. 2021.
- [26] M. R. Akdeniz, Y. Liu, M. K. Samimi, S. Sun, S. Rangan, T. S. Rappaport, and E. Erkip, "Millimeter wave channel modeling and cellular capacity evaluation," *IEEE J. Sel. Areas Commun.*, vol. 32, no. 6, pp. 1164–1179, Jun. 2014.
- [27] J. B. Kruskal, "Three-way arrays: rank and uniqueness of trilinear decompositions, with application to arithmetic complexity and statistics," *Linear algebra Appl.*, vol. 18, no. 2, pp. 95–138, 1977.
- [28] J. H. Conway, R. H. Hardin, and N. J. Sloane, "Packing lines, planes, etc.: Packings in grassmannian spaces," *Experimental mathematics*, vol. 5, no. 2, pp. 139–159, 1996.
- [29] L. De Lathauwer, "Decompositions of a higher-order tensor in block terms—part II: Definitions and uniqueness," *SIAM J. Matrix Anal. Appl.*, vol. 30, no. 3, pp. 1033–1066, 2008.
- [30] N. Vervliet, O. Debals, and L. De Lathauwer, "Tensorlab 3.0—numerical optimization strategies for large-scale constrained and coupled matrix/tensor factorization," in *Proc. 50th Asilomar Conf. Signals Syst. and Comput.* IEEE, 2016, pp. 1733–1738.
- [31] P. Paatero, "The multilinear engine—a table-driven, least squares program for solving multilinear problems, including the n-way parallel factor analysis model," *J. Computational Graphical Statist.*, vol. 8, no. 4, pp. 854–888, 1999.
- [32] D. Nion and L. De Lathauwer, "Levenberg-marquardt computation of the block factor model for blind multi-user access in wireless communications," in *Proc. 14th European Signal Process. Conf.* IEEE, 2006, pp. 1–4.
- [33] L. De Lathauwer and D. Nion, "Decompositions of a higher-order tensor in block terms—part III: Alternating least squares algorithms," *SIAM J. Matrix Anal. Appl.*, vol. 30, no. 3, pp. 1067–1083, 2008.
- [34] D. Love, R. Heath, and T. Strohmer, "Grassmannian beamforming for multiple-input multiple-output wireless systems," *IEEE Trans. Inf. Theory*, vol. 49, no. 10, pp. 2735–2747, Oct. 2003.
- [35] A. Medra and T. N. Davidson, "Flexible codebook design for limited feedback systems via sequential smooth optimization on the grassmannian manifold," *IEEE Trans. Signal Process.*, vol. 62, no. 5, pp. 1305–1318, Mar. 2014.
- [36] S. Sun, T. S. Rappaport, M. Shafi, P. Tang, J. Zhang, and P. J. Smith, "Propagation models and performance evaluation for 5G millimeter-wave bands," *IEEE Trans. Veh. Technol.*, vol. 67, no. 9, pp. 8422–8439, Sep. 2018.